The CWI pathway is activated through high hydrostatic pressure, enhancing glycerol efflux via the aquaglyceroporin Fps1 in *Saccharomyces cerevisiae*

Takahiro Mochizuki[*1], Toshiki Tanigawa[*1], Seiya Shindo[1], Momoka Suematsu[1], Yuki Oguchi[2], Tetsuo Mioka[1], Yusuke Kato[1], Mina Fujiyama[1], Eri Hatano[1], Masashi Yamaguchi[3], Hiroji Chibana[3], and Fumiyoshi Abe[1]†

[1]Department of Chemistry and Biological Science, College of Science and Engineering, Aoyama Gakuin University, 5-10-1 Fuchinobe, Chuo-ku, Sagamihara 252-5258, Japan

[2]Center for Instrumental Analysis, College of Science and Engineering, Aoyama Gakuin University, 5-10-1 Fuchinobe, Chuo-ku, Sagamihara 252-5258, Japan

[3]Medical Mycology Research Center, Chiba University, 1-8-1 Inohana, Chuo-ku, Chiba 260-8673, Japan.

Running title: High-pressure actives the CWI pathway to promote glycerol efflux via Fps1.

Keywords: *Saccharomyces cerevisiae*, high hydrostatic pressure, hypoosmotic stress, CWI pathway, Wsc1, Slt2, Fps1

Abbreviations: MPa, megapascals; CWI pathway, cell wall integrity pathway

*These authors contributed equally.

†To whom correspondence should be addressed:

Fumiyoshi Abe

Department of Chemistry and Biological Science, College of Science and Engineering, Aoyama Gakuin University, 5-10-1 Fuchinobe, Chuo-ku, Sagamihara 252-5258, Japan

Tel: +81-42-759-6233

E-mail: abef@chem.aoyama.ac.jp

Abstract

The fungal cell wall is the initial barrier for the fungi against diverse external stresses, such as osmolarity changes, harmful drugs, and mechanical injuries. This study explores the roles of osmoregulation and the cell wall integrity (CWI) pathway in response to high hydrostatic pressure in the yeast *Saccharomyces cerevisiae*. We demonstrate the roles of the transmembrane mechanosensor Wsc1 and aquaglyceroporin Fps1 in a general mechanism to maintain cell growth under high-pressure regimes. The promotion of water influx into cells at 25 MPa, as evident by an increase in cell volume and a loss of the plasma membrane eisosome structure, promotes the activation of Wsc1, an activator of the CWI pathway. The downstream mitogen-activated protein kinase Slt2 was hyperphosphorylated at 25 MPa. Glycerol efflux increases via Fps1 phosphorylation, which is initiated by downstream components of the CWI pathway and contributes to the reduction in intracellular osmolarity under high pressure. The elucidation of the mechanisms underlying adaption to high pressure through the well-established CWI pathway could potentially translate to mammalian cells and provide novel insights into cellular mechanosensation.

Introduction

Microorganisms encounter a wide variety of extreme environmental conditions, including heat, cold, salinity, or nutrient starvation. These stresses are first detected by sensor proteins that trigger the expression of specific genes via intracellular signaling pathways to respond to and overcome a crisis. Eukaryotes are also subjected to physical stresses, including tension, shear forces, and hydrostatic pressure. In mammalian cells, forces are detected, at the cell surface, through specific classes of integral membrane receptors, such as integrins and cadherins, which transduce stimuli into biochemical signals that initiate adaptive responses (Kechagia *et al.*, 2019; Ladoux and Mege, 2017). Unlike stretching or expansion, hydrostatic pressure acts on cells as a uniform stress and affects all substances and reactions in the cell, according to Pascal's principle. Therefore, it is difficult to identify sensors of high hydrostatic pressure and determine their effects on complex intracellular signaling networks. Nevertheless, there is ample evidence that cells modify their metabolism, transcription, translation, or post-translational processes in response to increasing hydrostatic pressure (Abe *et al.*, 1999; Abe, 2021; Bourges *et al.*, 2017; Hodder *et al.*, 2020; Iwahashi, 2015; Mishra *et al.*, 2022; Pattappa *et al.*, 2019).

Human cells also experience high hydrostatic pressures. In joints, cartilage is typically

59 subjected to hydrostatic pressures between 3–10 MPa (0.1 MPa = 1 bar = 0.9869 atm = 1.0197 kg/cm^2)
60 (Afoke *et al.*, 1987), with a maximum pressure of 18 MPa in the hip joint (Hodge *et al.*, 1989). The
61 loading of endothelial cells with a low pressure of 50 mmHg (~6.7 kPa) activates protein kinase C and
62 transiently activates the Ras/ERK pathway as a result of the water efflux through aquaporin 1 (Yoshino
63 *et al.*, 2020). High-pressure adaptation mechanisms in deep-sea microorganisms have also received
64 considerable attention. However, little is known regarding how microbial cells detect such stimuli and
65 convert them to intracellular signals.

66 Although *S. cerevisiae* is not a deep-sea piezophile, it can be used to elucidate the molecular
67 mechanisms underlying the cell's responses to high hydrostatic pressure by applying basic knowledge
68 of genetics and protein functions (Abe, 2021). Pressure pretreatment at a sublethal level (50 MPa for 1
69 h) increased the viability of yeast cells at 200 MPa, which is governed by two stress-induced
70 transcription factors, Msn2 and Msn4 (Domitrovic *et al.*, 2006). High pressure of 25 MPa accumulates
71 superoxide anions in mitochondria in a mutant deficient in superoxide dismutase 1 (Sod1), and the
72 mutant shows marked sensitivity to high pressures (Funada *et al.*, 2022). Incubation of yeast cells at 25
73 MPa for 5 h resulted in the upregulation of the *DAN/TIR* family mannoprotein genes, which are induced
74 under hypoxic conditions and at low temperatures (Abe, 2007). Target of rapamycin complex 1
75 (TORC1), an evolutionarily conserved serine/threonine kinase in eukaryotes, was activated by a
76 pressure of 25 MPa (Uemura *et al.*, 2020). We demonstrated that TORC1 plays a critical role in
77 maintaining an appropriate glutamine level under high pressure by downregulating the *de novo* synthesis
78 of glutamine (Uemura *et al.*, 2020). Such evidence indicates that high-pressure stress induces diverse
79 changes in intracellular processes and that cells survive by adaptively coping with each change. It may
80 appear that yeasts are not exposed to high hydrostatic pressure (equivalent to tens of MPa) on earth,
81 except for those inhabiting the deep sea. However, microorganisms inhabiting soil that are trampled by
82 a running 4 ton African elephant also experience comparable pressure. In addition, giant dinosaurs
83 weighing up to 100 tons roamed on the earth hundreds of millions of years ago, hence it must have been
84 crucial for soil microorganisms to acquire tolerance to extremely high pressure to survive during
85 evolution.

86 The fungal cell wall provides the first barrier against external stresses, such as osmolarity
87 changes, harmful drugs, and mechanical injuries. It is an elastic structure with a thickness of 50–500 nm
88 and is composed of β1,3-glucan, β1,6-glucan, chitin, and mannoproteins (Lesage and Bussey, 2006;

Levin, 2011; Orlean, 2012). The Young's modulus of the cell wall is estimated to be between 10 and 100 MPa (Davi *et al.*, 2019; Ma *et al.*, 2005), which is an intermediate value between that of low-density polyethylene and rubber. The primary mechanical role of the cell wall is to maintain cell morphology by balancing the tension generated by the turgor pressure, which is important for polarized cell growth (Bi and Park, 2012; Madden and Snyder, 1998; Pruyne and Bretscher, 2000). In *S. cerevisiae,* cell wall destabilization is sensed by transmembrane sensors of the WSC family (Wsc1, Wsc2, and Wsc3), as well as Mid2 and its homolog Mtl1 (Jimenez-Gutierrez *et al.*, 2020; Kock *et al.*, 2015; Levin, 2005; Levin, 2011; Philip and Levin, 2001), which activates a conserved signal transduction cascade, namely, the cell wall integrity (CWI) pathway. Their architecture is analogous to that of the mammalian transmembrane integrins (Elhasi and Blomberg, 2019). Among the five sensor proteins in *S. cerevisiae*, Wsc1 has been extensively studied both genetically and biophysically (Banavar *et al.*, 2018; Dupres *et al.*, 2009; Heinisch *et al.*, 2010; Merchan *et al.*, 2004; Neeli-Venkata *et al.*, 2021; Philip and Levin, 2001; Schoppner *et al.*, 2022). The CWI pathway in *S. cerevisiae* is activated in response to cell wall damage; however, recent evidence suggests that it is also involved in other stress conditions, indicating functional diversity (Banavar *et al.*, 2018; Cruz *et al.*, 2013; Kock *et al.*, 2016; Straede and Heinisch, 2007). To date, the effects of high hydrostatic pressure in yeast cells have not been studied with a focus on osmoregulation and the CWI pathway.

Atomic force microscopy (AFM) analysis revealed that a serine-threonine-rich (STR) domain has a nanospring-like structure that expands and contracts under external pressure, which in turn causes dephosphorylation of the cytoplasmic tail of Wsc1, transmitting signals downstream (Dupres *et al.*, 2009; Heinisch *et al.*, 2010; Vay *et al.*, 2004). The cytoplasmic tail of Wsc1 interacts with the GDP/GTP exchange factor Rom2, which subsequently activates small GTPase Rho1(Philip and Levin, 2001; Vay *et al.*, 2004). Bem2, Sac7, Lrg1, and Bag7 act as GTPase-activating proteins (GAPs) for Rho1 (Fig. 1)(Martin *et al.*, 2000; Peterson *et al.*, 1994; Schmidt *et al.*, 1997; Schmidt *et al.*, 2002). Rho1 regulates protein kinase C (Pkc1), a serine/threonine protein kinase that is essential for cell wall remodeling (Levin, 2011).

Pkc1 then activates three protein kinase-signaling modules that integrate the mitogen-activated protein kinase kinase kinase (MAPKKK) Bck1, redundant mitogen-activated protein kinase kinases (MAPKKs) Mkk1 and Mkk2, and mitogen activated protein kinase (MAPK) Slt2 (Levin, 2011). Slt2 kinase regulates many cellular processes, such as fine-tuning of the CWI pathway, transcriptional

119 response to cell wall damage, cell cycle progression, and nuclear export of mRNA (Gonzalez-Rubio *et*
120 *al.*, 2022), and mediates aquaglyceroporin Fps1 phosphorylation (Ahmadpour *et al.*, 2016; Levin, 2005;
121 Mollapour *et al.*, 2009). Although the CWI cascade is well characterized (Fig. 1), the exact mode of
122 Wsc1 action in response to different environmental cues remains unclear.

123 Fps1 is under the control of the CWI pathway (Ahmadpour *et al.*, 2016; Laz *et al.*, 2020). In
124 yeast, when the cell wall is damaged, water flows into the cell due to the osmotic pressure difference
125 between the inside and outside of the cell. To cope with this stress and prevent osmolysis, yeast cells
126 activate Fps1 to expel glycerol and eliminate osmotic pressure differences (Tamas *et al.*, 1999). The
127 opening and closing of Fps1 is a complex process mediated by protein phosphorylation involving several
128 signaling pathways (Fig. 1). First, MAP kinase Hog1 is activated in response to hyperosmotic stress and
129 phosphorylates the T231 residue of Fps1, resulting in Fps1 closure (Mollapour and Piper, 2007; Thorsen
130 *et al.*, 2006). Hog1 negatively regulates this channel by displacing the Fps1-activating proteins Rgc1
131 and Rgc2, thereby causing Fps1 closure (Lee *et al.*, 2013). Second, the open state of Fps1 requires
132 phosphorylation by Ypk1, a target of TORC2-dependent protein kinase (Muir *et al.*, 2015). Third, Fps1
133 and Slt2 physically interact via phosphorylation of the S537 residue of Fps1, which promotes the
134 opening of the glycerol channel (Ahmadpour *et al.*, 2016).

135 Remarkably, while imaging wild-type *S. cerevisiae* cells, minor cell swelling was observed
136 after high-pressure incubation at 25 MPa. This suggests that high pressure may facilitate the influx of
137 water into the cell or damage the cell wall, further allowing water influx. This observation steered us to
138 study high-pressure signaling, with a focus on water influx, turgor pressure, the CWI pathway via Wsc1,
139 MAP kinase Slt2, and aquaglyceroporin Fps1 (Fig. 1). Our study provides novel insights into the
140 signaling events triggered by the application of high-pressure and the resulting molecular mechanisms
141 that help cells to cope with such stress.

142

143 **Results**

144 **Wsc1 is required for efficient cell growth under high pressure**

145 Based on the previous studies (Jimenez-Gutierrez *et al.*, 2020; Kock *et al.*, 2015; Levin, 2005; Levin,
146 2011; Philip and Levin, 2001), we hypothesized that any of the five sensor proteins, Wsc1–3, Mid2, and
147 Mtl1, could detect hydrostatic pressure changes, either directly or as a result of cell wall damage, and
148 activate the CWI pathway to allow for high-pressure growth. Cells were cultured in synthetic complete

149 (SC) medium at an OD_{600} of 0.01 for 48 h, under atmospheric pressure (0.1 MPa) or 25 MPa. We found
150 that the *wsc1*Δ mutant exhibited a moderate growth defect at 25 MPa, whereas the other mutants grew
151 as efficiently as the wild-type cells (Fig. 2A). The result suggests that Wsc1 plays a primary role in high-
152 pressure growth, while the other sensor proteins may contribute to the growth with overlapping functions.
153 Wsc1 is characterized by an N-terminal extracellular cysteine-rich domain (CRD), followed
154 by a glycosylated STR domain, a single transmembrane domain, and a C-terminal cytoplasmic tail,
155 which is considered to be the mechanosensory region (Fig. 1). The CRD and STR domains detect
156 structural changes in the cell wall (Dupres *et al.*, 2009; Heinisch *et al.*, 2010). An alanine substitution
157 of eight cysteines in the CRD of Wsc1 had a marginal effect on high-pressure growth ability, whereas
158 deletions of the STR and the entire N-terminal region caused sensitivity to high pressure (Fig. 2B).
159 These results suggest that the STR of Wsc1 can detect structural changes in the cell wall caused by high
160 pressure.
161 Single-molecule AFM results indicated that Wsc1 assembles in patches as large as 200 nm on
162 the plasma membrane, thereby enhancing transduction of the CWI signaling pathway (Dupres *et al.*,
163 2009; Heinisch *et al.*, 2010). Wsc1 assembles at the tips and bud necks where cells undergo polar growth,
164 and endocytosis is essential for their polarity (Piao *et al.*, 2007). To determine the effect of high pressure
165 on the distribution of Wsc1, we observed the localization of Wsc1-GFP before and after culturing the
166 cells at 25 MPa. Cells were observed after depressurization. As previously reported (Piao *et al.*, 2007;
167 Wilk *et al.*, 2010), Wsc1-GFP localized mainly to bud tips, but also to the plasma membrane of mother
168 cells as patchy structures, and possibly to late endosomes as punctate structures and vacuoles (Fig. 2C).
169 The bud tip localization of Wsc1-GFP was maintained after the high-pressure incubation although its
170 vacuolar degradation was slightly enhanced (Fig. 2C). Enhanced vacuolar degradation of membrane
171 proteins under high pressure has also been observed in the tryptophan permeases Tat1 and Tat2 (Abe
172 and Iida, 2003; Suzuki *et al.*, 2013). The overall localization of GFP-tagged $Wsc1^{8C>A}$, $Wsc1^{STR\Delta}$, and
173 $Wsc1^{Nter\Delta}$ was comparable with the wild-type Wsc1-GFP (Fig. 2D). The polarized distribution of Wsc1
174 to bud tips requires endocytosis (Piao *et al.*, 2007; Wilk *et al.*, 2010). The Wsc1 mutant, in which the
175 NPF sequence at the C-terminal tail was replaced by AAA, exhibited a uniform distribution of Wsc1
176 within the plasma membrane (Piao *et al.*, 2007). $Wsc1^{NPF>AAA}$-GFP was present throughout the plasma
177 membrane (Fig. 2C) and $Wsc1^{NPF>AAA}$ expressing cells grew as efficiently as the wild-type cells at 25
178 MPa (Fig. 2B). Therefore, we suggest that Wsc1 is required for efficient cell growth under high pressure

179 but does not need to be exclusively localized to the bud tips.

180

181 **Wsc1 activates the CWI pathway in response to high pressure**

182 To address the role of Wsc1 in optimal growth under high pressure, we focused on the downstream
183 effector Rom2. The Wsc1 C-terminal cytoplasmic domain residue, Y303, is critical for its interaction
184 with Rom2 (Vay *et al.*, 2004). Both the disruption of *ROM2* and the Wsc1-Y303A mutation, which
185 interferes with the Wsc1–Rom2 interaction, resulted in growth defects at 25 MPa (Fig. 3A). Among the
186 four Rho1 GAP genes, deletions in *BEM2, SAC7*, and *LRG1* caused growth defects at 25 MPa to varying
187 degrees (Fig. 3A). The expression of GTP-bound active forms of Rho1-F35L or Q68H failed to restore
188 the high-pressure sensitivity of the *rom2*Δ mutant (Fig. 3B), suggesting that the association of Rho1
189 with Rom2 is critically important for high-pressure growth. The expression of the constitutively active
190 form of Pkc1-R398P allowed the *rom2*Δ mutant to grow efficiently at 25 MPa (Fig. 3B). Disruption of
191 *PKC1*, *BCK1*, or *SLT2* resulted in severe high-pressure sensitivity, whereas only disruption of *MKK1*,
192 and not *MKK2*, caused moderate high-pressure sensitivity (Fig. 3C). These results suggest that Wsc1
193 acts as a mechanosensor that detects hydrostatic pressure changes and may transmit the pressure signal
194 into the CWI pathway.

195 To validate this hypothesis, we assessed the phosphorylation of Slt2 in response to high
196 pressure and found it to increase in a pressure-dependent manner, suggesting that high pressure activates
197 the CWI pathway (Fig. 3D). Also, disruption of *WSC1* reduced the phosphorylation level of Slt2 by 60%
198 at 25 MPa compared with the wild-type level. This indicates that other proteins, such as Mid2, may also
199 activate the CWI pathway in response to pressure (Fig. 3E). In contrast, loss of *BCK1* resulted in a
200 complete loss of Slt2 phosphorylation (data not shown).

201 Slt2 is under the control of the CWI signaling pathway, which is responsible for maintaining
202 cell wall homeostasis (Gonzalez-Rubio *et al.*, 2022; Levin, 2005; Martin *et al.*, 2000). Thus,
203 hyperphosphorylated Slt2 may modulate the transcription of downstream genes through
204 phosphorylating its substrates under high pressures. To verify this, we analyzed the effect of high
205 pressure on the localization of Swi4, one of the downstream transcription factors of Slt2. Wild-type cells
206 that express Swi4-GFP were incubated with 15 μg/mL nocodazole in a YPD medium for 2 h at 0.1 MPa
207 to induce cell cycle arrest in the G_2/M phase (Kim *et al.*, 2010) when most of the Swi4-GFP was present
208 in the cytoplasm. Synthetic Complete (SC) medium was not used in this analysis because nocodazole

209 was ineffective in arresting the cell cycle even at higher concentrations (data not shown). Cells were
210 then cultured for 5 h at 0.1 MPa or 25 MPa. We found that the percentage of cells with Swi4-GFP
211 migrating from the cytoplasm to the nucleus was higher at 25 MPa (46%, n > 300) than at 0.1 MPa
212 (17%, n > 300) (Fig. 4A). Furthermore, cells lacking Swi4 or Swi6 showed marked high-pressure
213 sensitivity (Fig. 4B). These results support our model, which confirms that high pressure activates the
214 CWI pathway.
215
216 **High pressure facilitates water influx into the cells**
217 While conducting this study, we noticed that the wild-type cells were moderately swollen after
218 incubation at 25 MPa. To validate this further, we examined whether the distribution of eisosomes was
219 affected by pressure. Eisosomes, peripheral membrane protein complexes located on the cytoplasmic
220 side of membrane compartments occupied by Can1 (MCC), are membrane invaginations (Douglas and
221 Konopka, 2014; Lanze *et al.*, 2020; Sakata *et al.*, 2022). If the cell swells and the plasma membrane
222 undergoes stretching under high pressure, the membrane invaginations should disappear. To verify this,
223 we observed cells co-expressing the low-affinity tryptophan permease Tat1-GFP as a plasma membrane
224 marker (Ishii *et al.*, 2022; Suzuki *et al.*, 2013) and an eisosome resident protein, Nce102-mCherry, after
225 cultured at 25 or 50 MPa. Cells were observed at 0.1 MPa within 15 min of depressurization. At 0.1
226 MPa, Nce102-mCherry was localized to the plasma membrane in a patchy pattern characteristic of
227 eisosomes (Fig. 5A). Notably, after high-pressure culture at 25 or 50 MPa, Nce102-mCherry was evenly
228 distributed within the plasma membrane (Fig. 5A). This was partially suppressed by the presence of 1
229 M sorbitol (Fig. 5A). When the co-localization of Tat1-GFP and Nce102-mCherry was examined at the
230 cell surface, Pearson's correlation coefficient (PCC) increased with incubation time at 25 MPa (Fig. 5B),
231 confirming the even distribution of Nce102 under high pressure. Similar increases in PCC with Tat1
232 were found for Pil1 and Sur7, another two eisosome-associated proteins, but not as pronounced as for
233 Nce102 (Fig. 5B). These results suggest that the influx of water into the cells after high-pressure
234 incubation results in tension in the plasma membrane. In the *wsc1*Δ and *slt2*Δ mutants, Nce102-mCherry
235 was not localized in a patchy pattern but was more evenly distributed within the plasma membrane even
236 under 0.1 MPa, suggesting excess water influx (data not shown).
237 Next, the cell volume was calculated by measuring the cell diameter using Tat1-GFP as the
238 plasma membrane marker. We found that the cell volume increased 1.2-fold after incubation at 25 MPa

239 or 50 MPa for 1 or 3 h, suggesting that water influx occurred under high pressure (Fig. 5A, B). To verify
240 pressure-induced cell swelling, we examined the effects of 1 M sorbitol addition on cell volume under
241 high pressure. As expected, 1 M sorbitol suppressed the high pressure-induced increase in cell volume
242 (Fig. 5C). If high pressure merely pushed water into cells, the cell size would be restored following
243 depressurization. However, the above results show that the cells remain swollen 15 min post
244 depressurization until microscopic observation at atmospheric pressure. Therefore, even 1 h of
245 incubation at 25 or 50 MPa would have caused irreversible changes to the cell wall. However, it remains
246 unclear whether a high-pressure load directly weakens the cell wall structure or the cell wall expanded
247 irreversibly due to increased water influx into the cell due to high-pressure application. In any case, cells
248 were at higher risk of rupture under high pressure; therefore, to cope with this, cells tend to prevent
249 water influx by expelling glycerol, the major osmolyte in yeast, to reduce internal osmotic pressure.
250 Therefore, we focused on the regulation of intracellular glycerol levels under high hydrostatic pressure.
251

252 **Aquaglyceroporin Fps1-mediated glycerol efflux is required for high-pressure growth**

253 Under hyperosmotic conditions, yeast cells synthesize or retain high concentrations of glycerol to
254 maintain their osmotic balance (Blomberg, 2022; de Nadal and Posas, 2022; Hohmann, 2002).
255 Intracellular glycerol concentration is partially regulated by Fps1, an aquaglyceroporin on the plasma
256 membrane. Fps1 closes when extracellular osmolarity is high and opens when it is low, to expel glycerol
257 and prevent cell rupture (Ahmadpour *et al.*, 2016; Beese *et al.*, 2009; Lee *et al.*, 2013; Luyten *et al.*,
258 1995; Muir *et al.*, 2015). The growth of the *fps1*Δ mutant was sensitive at 25 MPa (Fig. 6A). The addition
259 of 1 M sorbitol to the medium restored the growth of the *fps1*Δ mutant to the wild-type level, at 25 MPa
260 (Fig. 6A). Disruption of the glycerol synthase genes *GPP1* or *GPD1* increased, albeit partially, the high-
261 pressure growth ability of the *fps1*Δ mutant (Fig. 5C). Furthermore, single deletion of *GPP1* enhanced
262 high-pressure growth in the wild-type strain, although deletion of other glycerol biosynthetic genes had
263 no promotive effect (Fig. 6B).

264 Next, we analyzed the intracellular and extracellular glycerol concentrations. Wild-type and
265 *fps1*Δ cells in SC medium were incubated at 0.1 MPa and 25 MPa for 24 h, starting with an initial OD_{600}
266 of 0.1. Upon analyzing these cells, we found that the intracellular glycerol concentration in wild-type
267 cells decreased markedly after high-pressure culture, whereas more glycerol accumulated extracellularly
268 (Fig. 6C). By contrast, *fps1*Δ cells had a 3-fold higher intracellular glycerol concentration than wild-

269 type cells, which remained unchanged even after high-pressure culture (Fig. 6C). Thus, we concluded
270 that wild-type cells expelled glycerol via Fps1 to cope with the high-pressure-induced excess water
271 influx.

272 Furthermore, the ultrastructure of cells via transmission electron microscopy (TEM) showed
273 that wild-type cells underwent no significant changes in cell morphology or cell wall structure after
274 incubation at 25 MPa (Fig. 7). The ultrastructure of *fps1*Δ cells also appeared normal at 0.1 MPa.
275 Interestingly, 20–40% of *fps1*Δ cells had sharply ruptured cell walls, without any abnormalities in their
276 intracellular structures at 25 MPa (Fig. 7, arrows). The *fps1*Δ cell wall is weakened by increased turgor
277 pressure due to glycerol accumulation; high pressure might also have caused further damage to the cell
278 wall, leading to cell rupture.

279

280 **Fps1 opening is likely regulated by Slt2 during high-pressure cultures**

281 The upstream regulators of Fps1 were analyzed to determine the mechanism by which cells regulate
282 Fps1 in response to high pressure. Previous studies have indicated that Hog1 is a negative regulator of
283 Fps1 opening, whereas Ypk1 and Slt2 are positive regulators (Fig. 1)(Ahmadpour *et al.*, 2016; Lee *et*
284 *al.*, 2013; Muir *et al.*, 2015). To determine which kinases are involved in the regulation of the Fps1 in
285 response to high pressure, we examined the high-pressure growth ability of the *fps1*Δ mutant expressing
286 Fps1-T231A (Hog1 target site) or S537A (facilitates binding with Slt2) at 25 MPa. We found that the
287 Fps1-S537A strain showed high sensitivity, whereas the Fps1-T231A strain, as well as the wild-type
288 strain, grew at 25 MPa (Fig. 8A). We examined the phosphorylation of Fps1 using western blotting and
289 observed a high-molecular-weight band of Fps1-3HA, the intensity of which increased slightly (2.2 ±
290 0.3-fold, n = 3) with increasing pressure at 25 MPa (Fig. 8B). As expected, the high molecular weight
291 band of Fps1-3HA disappeared in cells expressing Fps1-S537A (Fig. 8B). Phosphorylation of the S537
292 residue of Fps1 is essential for its interaction with Slt2; however, there is no evidence of its direct
293 phosphorylation by Slt2 (Ahmadpour *et al.*, 2016).

294 The *slt2*Δ mutant was particularly sensitive to high pressure (Fig. 3C, 8C), which was
295 completely rescued by the addition of 1M sorbitol (Fig. 8C). Therefore, the high-pressure sensitivity of
296 the *slt2*Δ mutant was attributed to the excess water influx, at least in part, owing to its inability to open
297 Fps1 and expel glycerol. The *hog1*Δ mutant also showed high-pressure sensitivity although the Fps1-
298 T231A mutant grew at 25 MPa (Fig. 8A). The result suggests that Hog1 plays a role other than the Fps1

299 regulation under high pressure (Fig. 8C). The addition of 1M sorbitol did not restore high-pressure
300 growth ability of the *hog1*Δ, *swi4*Δ, and *swi6*Δ mutants (Fig. 8C). Interestingly, Slt2 was also
301 hyperphosphorylated when cultured with 1 M sorbitol at 25 MPa where there is no excessive influx of
302 water into cells (Fig. 8D). The result suggests that the activation of the CWI pathway by high pressure
303 may also be caused by a direct effect of high pressure on Wsc1, in addition to its activation via the cell
304 swelling associated with the excessive influx of water under high pressure.

305 To verify whether the high-pressure sensitivity of the *slt2*Δ mutant was due to reduced Fps1
306 activity, we expressed $Fps1^{S537E}$, a simulated phosphorylated form of Fps1 at the S537 residue, and found
307 that it efficiently rescued the high-pressure sensitivity of the *slt2*Δ mutant (Fig. 8E). Therefore, Slt2
308 activates Fps1, thereby preventing water influx and allowing for cell growth under high pressure. Given
309 that 1 M sorbitol fully restored the high-pressure growth ability of the *slt2*Δ mutant (Fig. 8C), it is
310 possible that Slt2 may also prevent water influx under high pressure by another mechanism, in addition
311 to activating Fps1.

312

313 **Ypk1 is required for growth under high pressure, independent of the regulation of Fps1**

314 Fps1 is also phosphorylated by Ypk1 for its activation, depending on TORC2 signaling (Muir
315 *et al.*, 2015). We found that the disruption of *YPK1* caused a severe defect in cell growth at 25 MPa,
316 demonstrating the importance of Ypk1 (Fig. 8F). Ypk1 is phosphorylated by multiple protein kinases
317 such as Fpk1/Fpk2 (Rispal *et al.*, 2015), Pkh1/Pkh2 (Roelants *et al.*, 2002; Roelants *et al.*, 2004;
318 Roelants *et al.*, 2010), and TORC2 (Leskoske *et al.*, 2017; Muir *et al.*, 2015; Roelants *et al.*, 2004) (Fig.
319 1). To infer which kinases are required for high-pressure growth via phosphorylation of Ypk1, we
320 examined the effect of alanine substitutions for S51/S57 residues (Fpk1/Fpk2 target sites for Ypk1
321 inactivation), T504 residue (Pkh1/Pkh2 target site for Ypk1 activation), and S644/T662 residues
322 (TORC2 target sites for Ypk1 activation) on cell growth under high pressure (Fig. 1). While cells
323 expressing Ypk1-S51A-S71A grew as efficiently as wild-type cells at 25 MPa, those expressing Ypk1-
324 T504A or S644A-T662A showed severe growth defects under the pressure (Fig. 8F). Thus, it is possible
325 that Pkh1/Pkh2 and/or TORC2 phosphorylate Ypk1 in response to high pressure. As shown in Fig. 4,
326 cells swelled after high-pressure incubation, and the eisosome structure disappeared. This raises the
327 possibility that Slm1, localized in the eisosome, is released by high pressure and eventually binds to and
328 activates TORC2, ultimately phosphorylating Ypk1 (Fig. 1)(Berchtold *et al.*, 2012; Riggi *et al.*, 2018).

329 To test this hypothesis in our preliminary experiments, Lsp1-mCherry/Slm1-GFP-co-expressing and
330 Avo3-3×mCherry/Slm1-GFP-co-expressing strains were constructed, and any alterations in the
331 colocalization of each strain under high pressure were observed using confocal laser microscopy. Avo3
332 and Lsp1 are components of TORC2 and the eisosome, respectively (Babst, 2019; Eltschinger and
333 Loewith, 2016). We found that the colocalization of Lsp1-mCherry and Slm1-GFP decreased after cell
334 incubation at 25 MPa, whereas that of Avo3-3×mCherry and Slm1-GFP appeared to increase, suggesting
335 TORC2 activation (Fig. S1A). Furthermore, phospho-Ypk1 was detected using a rabbit monoclonal
336 antibody for phospho-PKC (pan) (zeta Thr410) (190D10), which reacts with the phosphorylated T504
337 residue, and after incubation at 25 MPa for 3 h, its phosphorylation level increased 7-fold. (Fig. S1B).
338 To test whether phosphorylation of Fps1 by Ypk1 is required for high-pressure growth, the
339 effect of phosphorylation site mutations was examined. Residue S570 of Fps1 is majorly phosphorylated
340 by Ypk1, while the phosphorylation of residues S181 and S185 has also been reported (Fig. 1) (Muir *et*
341 *al.*, 2015). Both the Fps1-S570A-substituted and S181A-S185A-S570A triple-substituted strains grew
342 as well as the wild-type strain (Fig. 8G). Consistent with this result, the electrophoretic mobility of the
343 alanine substitution mutants Fps1-S570A-3HA, Fps1-A181A-S185A-3HA, and Fps1-A181A-S185A-
344 S570A-3HA remained unaffected (Fig. 8B). Thus, Ypk1 is unlikely to phosphorylate Fps1 in response
345 to high pressure.
346
347 **Discussion**
348 Based on the coincidental observation that cells moderately swell under high pressure, the importance
349 of glycerol efflux by Fps1 and its regulation via the CWI pathway has been the focus of this study. We
350 propose the presence of high-pressure signaling systems mediated by the stress sensor Wsc1 (Fig. 9). In
351 our model, high pressure activates the CWI pathway in two distinct modes. First, high pressure promotes
352 water influx into yeast cells, thereby increasing turgor pressure, which in turn expands the cell walls and
353 activates Wsc1 (Fig. 2–5). Second, high pressure directly activates Wsc1, as suggested by our finding
354 that Slt2 was hyperphosphorylated at 25 MPa even in the absence of cell swelling in 1 M sorbitol
355 medium (Fig. 8D). From the first perspective, the water influx caused by increased hydrostatic pressure
356 is similar to that of hypoosmotic stress. In growing yeast cells, turgor pressure is estimated to be 0.5–
357 1.5 MPa due to the influx of water driven by the osmotic gradient (Atilgan *et al.*, 2015; Minc *et al.*,
358 2014; Mishra *et al.*, 2022; Schaber *et al.*, 2010). The turgor pushes the cell membrane, further expanding

359 the cell wall. Using an osmometer, we found the osmotic pressure of the SC medium to be 255 ± 0
360 mOsm/kg (n = 3), which corresponds to 0.588 MPa (nearly 0.6 MPa). Assuming that the turgor pressure
361 of the cells was 1.0 MPa, the intracellular osmotic pressure was 1.6 MPa. Applying hydrostatic pressure
362 to the cell culture caused a water influx into the cells until the water potentials inside and outside the
363 cell became equivalent. Conversely, from the second perspective, it is possible that high pressure of 25
364 MPa directly modulates Wsc1 structure or promotes physical interaction between Wsc1 and Rom2;
365 however, evidence of high pressure-induced structural changes in Wsc1 or enhanced Wsc1–Rom2
366 interaction under high pressure remains lacking.

367 High pressure may also cause some perturbation to the cell wall, as suggested by our
368 observations that cells remain swollen at least 15 min post depressurization (Fig. 5). However, there is
369 currently no direct evidence that high pressures of 25 MPa damage cell walls. Since high hydrostatic
370 pressure has little effect on covalent binding (Chen *et al.*, 2017), it is unlikely that the β1,3-glucan or
371 β1,6-glucan networks are cleaved by high pressure. Rather, we suspect that pressure may have a greater
372 effect on the levels of cell wall mannoproteins. Our previous DNA microarray results showed that
373 transcription of the gene encoding for the major cell wall mannoprotein Cwp1 was markedly reduced
374 under 25 MPa; instead, the *DAN/TIR* family mannoprotein genes, which are typically induced under
375 hypoxic conditions (Abramova *et al.*, 2001), were significantly enhanced (Abe, 2007). Although their
376 protein levels have not been examined, the composition of mannoproteins may change with high
377 pressure, and eventually, cell wall elasticity may change. Once the CWI pathway is activated, Slt2 kinase
378 promotes glycerol efflux through aquaglyceroporin Fps1, thereby allowing for cells to expel glycerol
379 and adjust the osmotic pressure balance across the plasma membrane (Fig. 6). Under high pressure, the
380 high molecular weight band of Fps1 increased, suggesting enhanced Fps1 phosphorylation. However, a
381 similar high molecular weight band of Fps1 was also observed in the *slt2*Δ mutant, although it
382 disappeared in $Fps1^{S537A}$. This suggests other kinases besides Slt2 that phosphorylate the Fps1 S537
383 residue. Since phosphorylation of Fps1 S537 residues is critical for binding to Slt2, there may be other
384 sites of authentic phosphorylation by Slt2. The role of Slt2 in growth under high pressure is not only
385 limited to the activation of Fps1, but also the phosphorylation of Swi4/Swi6 and the induction of
386 transcription of many downstream genes. This is justified by the fact that loss of *SWI4* or *SWI6* causes
387 severe high-pressure sensitivity (Fig. 4).

388 As per the TEM images of *fps1*Δ cells, the cell wall ruptured sharply after a high-pressure

389 incubation (Fig. 7). This observation may be due to the localized weakening of the cell wall by increased
390 turgor pressure due to glycerol accumulation in the *fps1*Δ cells. High pressure may have caused further
391 damage to the cell wall in the *fps1*Δ mutant, leading to cell rupture. However, we cannot rule out the
392 possibility that the weakened *fps1*Δ cell walls were ruptured during TEM sample preparation by the
393 sandwich freezing method (Yamaguchi *et al.*, 2021a; Yamaguchi *et al.*, 2021b).

394 Although this study showed the importance of Ypk1 kinase in high-pressure growth (Fig. 8F),
395 it did not provide evidence that Ypk1 regulates the opening of Fps1 by phosphorylation (Fig. 8G). Rather,
396 alanine substitutions at Ypk1 residues, phosphorylated by TORC2 and Pkh1/Pkh2 kinases, prevented
397 high-pressure growth (Fig. 8F). TORC2-Ypk1 regulates polarization of the actin cytoskeleton and
398 sphingolipid biosynthesis (Kamada *et al.*, 2005; Rispal *et al.*, 2015; Roelants *et al.*, 2011; Tabuchi *et al.*,
399 2006). Therefore, the regulation of sphingolipid synthesis or actin organization may be important for
400 high-pressure adaptation. Indeed, high pressures stiffen membrane lipid bilayers (Matsuki *et al.*, 2013;
401 Winter, 2002), which may adversely affect membrane protein functions, membrane fusion, or membrane
402 trafficking. Furthermore, hypoosmotic stress causes the depolymerization of the actin cytoskeleton
403 (Gualtieri *et al.*, 2004). To cope with these pleiotropic effects of high pressure, yeast cells may activate
404 Fps1 via the CWI pathway to expel glycerol and avoid cell rupture, promote sphingolipid synthesis via
405 the TORC2-Ypk1 pathway to maintain membrane homeostasis, and regulate actin cytoskeleton
406 organization.

407 Therefore, the regulation of sphingolipid synthesis and actin cytoskeleton via the TORC2-
408 Ypk1 pathway is an interesting research target for understanding the physiological responses to high
409 hydrostatic pressure in yeast.

410 Our previous studies have shown that defects in *TRP1*, *TAT2*, TORC1-EGOC, or poorly
411 characterized genes such as *EHG1/MAY24* cause severe high-pressure sensitivity (Abe and Horikoshi,
412 2000; Abe and Minegishi, 2008; Kurosaka *et al.*, 2019; Uemura *et al.*, 2020). On the contrary, the defects
413 in the CWI pathway and Fps1 shown in this study caused relatively mild sensitivity to high-pressure.
414 This is probably because the former defects cause impaired nutrient uptake or aberrant glutamine
415 accumulation under 25 MPa, resulting in rapid growth arrest after pressurization, whereas the latter
416 defects are due to an inability to prevent water influx under high pressure, which causes the negative
417 effects on growth to progress slowly. Yeasts possess two types of aquaporins, Aqy1 and Aqy2. However,
418 both alleles are nonfunctional in experimental strains derived from S288C, such as strain BY4742 (Sabir

419 *et al.*, 2017). Therefore, the water influx into the cell when exposed to hypoosmotic or high hydrostatic
420 pressure stress is thought to be mainly due to passive diffusion across the plasma membrane lipid
421 bilayers. Passive diffusion of water across the lipid bilayer is much slower than water flux through
422 aquaporins. This could explain why the effects of high-pressure stress are relatively mild. The Σ1278b
423 strain and the naturally occurring *S. cerevisiae* strains have functional *AQY* alleles (Laize *et al.*, 1999).
424 Therefore, the effects of hypoosmotic and high-pressure stress in these strains could be more severe than
425 in the experimental strains. The osmotic pressure of the SC medium was 255 mOsm/kg, which
426 corresponds to 127.5 mM NaCl. When it rains, the ambient osmotic pressure drops to near zero,
427 exposing naturally occurring yeasts to greater hypoosmotic stress. Exposure to high hydrostatic pressure
428 under such low osmotic pressure would pose a threat to their survival.
429 Meanwhile, the ambient osmotic pressure is isotonic for human and other animal cells.
430 Therefore, excessive water influx due to high water pressure loading, as observed in yeast in this study,
431 would not occur. However, when human endothelial cells are subjected to a pressure of 50 mmHg (~6.7
432 kPa), which corresponds to a transient increase in blood pressure during exercise, water is extruded from
433 the cell via aquaporin 1, causing cell contraction and plasma membrane deformation (Yoshino *et al.*,
434 2020). Consequently, protein kinase C is activated via the G protein-coupled receptor and phospholipase
435 C, which in turn activates the Ras/ERK pathway, ultimately leading to the formation of complex tubular
436 vascular structures (Yoshino *et al.*, 2020).
437 Since aquaporins are channels, if the water potential is equivalent inside and outside the cells, no water
438 efflux should occur even when the pressure is 50 mmHg. However, because the pressure is very weak,
439 the pressure applied at different sites in a single cell may be different, and water may be extruded through
440 aquaporins at lower-pressure sites.
441 The effects of high hydrostatic pressure vary not only with the magnitude of the applied
442 pressure but also with the duration of the pressurization. Therefore, the effects on the complex metabolic
443 processes of living cell systems cannot be generalized. The full picture of pressure effects will be
444 revealed by applying the extensive knowledge of yeast cell biology and sophisticated molecular genetic
445 tools to advanced transcriptomics, proteomics, and metabolomics studies, which could potentially be
446 translated to mammalian cells and help improve cellular health under normal and stress conditions.
447
448 **Materials and methods**

449 **Yeast strains and media**

450 The parental wild-type strain BY4742 and the deletion mutants used in this study are listed in Table 1.
451 Strains DL376 (*pkc1*Δ) and DL100 (the parental strain of DL376) were kindly provided by Dr. David
452 Levin of Boston University Goldman School of Dental Medicine through Dr. Hidetoshi Iida of Tokyo
453 Gakugei University (Levin and Bartlett-Heubusch, 1992). The two strains were transformed with
454 YCplac22 (*TRP1, CEN*) to provide tryptophan prototrophy. Cells were grown in SC medium or YPD
455 medium at 25 °C under 0.1 MPa or 25 MPa (Abe and Minegishi, 2008). The SC medium contained
456 0.67% yeast nitrogen base without amino acids (Becton, Dickinson and Company, MD, USA), 2% D-
457 glucose, 20 μg/mL methionine, 90 μg/mL leucine, 30 μg/mL isoleucine, 40 μg/mL tryptophan, 20
458 μg/mL histidine, 30 μg/mL lysine, 20 μg/mL methionine, 50 μg/mL phenylalanine, 30 μg/mL tyrosine,
459 20 μg/mL arginine, 100 μg/mL aspartic acid, 100 μg/mL glutamic acid, 400 μg/mL serine, and 200
460 μg/mL threonine. YPD medium contains 1% Bacto yeast extract (Becton, Dickinson and Company),
461 2% Bacto peptone (Becton, Dickinson and Company), and 2% D-glucose.

462

463 **High-pressure cell culture**

464 For most experiments examining growth efficiency under high pressure, growing cells in shaking culture
465 were diluted in SC or YPD medium to an OD_{600} of 0.01. The diluted cells were transferred to sterile 2.2-
466 mL tubes and sealed with Parafilm™ (Bemis Corp., Neenah, WI, USA). The tubes were placed in a 500-
467 mL high-pressure chamber (Abe and Minegishi, 2008) and subjected to 25 MPa at 25 °C for 48 h. After
468 depressurization, cell growth was evaluated by measuring OD_{600} using a PD-303 spectrophotometer
469 (Apel, Kawaguchi, Japan). Here, $OD_{600} = 1.0$ corresponds to 1.65×10^7 cells/mL in our device setup.

470

471 **Generation of plasmids and mutant strains**

472 The plasmids used in the present study are listed in Table 2. Polymerase chain reaction (PCR)-based
473 site-directed mutagenesis was performed using the appropriate primers. The primer sequences will be
474 disclosed upon reasonable request. Homologous recombination, using pJT6 (GFP, *HIS3*) and pJT601
475 (mCherry, *URA3*), was used to tag genes in the yeast genome with GFP and mCherry, respectively (kind
476 gifts from Dr. Jiro Toshima of Tokyo University of Science, (Kawada *et al.*, 2015)). Plasmids encoding
477 HA-Rho1 (SP333; *LEU2, CEN*), HA-Rho1^{F35L} (SP335; *LEU2, CEN*), and HA-Rho1^{Q68H} (SP336; *LEU2,*
478 *CEN*) were kindly provided by Dr. Satoshi Yoshida of Waseda University (Yoshida *et al.*, 2009). pBSK-

479 *SFK1*-3×mCherry-*CaURA3* was kindly provided by Dr. Takuma Kishimoto of Hokkaido University
480 Graduate School of Life Science (Kishimoto *et al.*, 2021). To generate Avo3-3×mCherry strain, a DNA
481 fragment encoding a *C*-terminal domain of Avo3 was amplified by PCR and was inserted into pBSK-
482 *SFK1*-3×mCherry-*CaURA3* of which *SFK1* gene had been removed. The resulting plasmid was
483 linearized by digestion with *Eco*RV and introduced into the wild-type strain harboring *SLM1*-GFP in the
484 genome.
485
486 **Western blotting**
487 Whole-cell extract preparation was performed as previously described (Ishii *et al.*, 2022). Briefly, 1.65
488 × 10^8 cells were collected by centrifugation; serially washed with 10 mM NaN_3, 10 mM NaF, and lysis
489 buffer A (50 mM Tris-HCl, 5 mM EDTA, 10 mM NaN_3, and Complete™ EDTA-free tablet; Roche
490 Diagnostics, Mannheim, Germany); disrupted with glass beads at 4 °C. Unbroken cells and debris were
491 removed by centrifugation at 900 × *g* for 5 min, and purified lysates were treated with 5% (w/v) Sodium
492 dodecyl sulfate (SDS) and 5% (v/v) 2-mercaptoethanol at 37 °C for 10 min. Whole-cell extract
493 preparation to detect phospho-Slt2 was performed as previously described (Wilk *et al.*, 2010) with some
494 modifications. Yeast cells amounting to 5 × 10^7 in SC medium were treated with 255 mM NaOH–1% 2-
495 mercaptoethanol on ice for 15 min, then 6% trichloroacetic acid (TCA) was added and cells were kept
496 on ice for another 15 min. The cell pellet was collected after centrifugation at 15,000 × *g* for 5 min,
497 washed with 1 M Tris-HCl (pH 6.8), and was treated with a sample buffer (65 mM Tris [pH6.8], 2%
498 SDS, 10% Glycerol, 100 mM DTT, 0.002% BPB) to denature proteins at 95 °C for 5 min. The
499 supernatant after centrifugation at 15,000 × *g* for 5 min was used for western blotting. Whole-cell extract
500 preparation to detect phospho-Ypk1was performed as previously described (Roelants *et al.*, 2011) with
501 some modifications. Yeast cells amounting to 1.65 × 10^7 were collected by centrifugation at 6,000 × *g*
502 for 1 min. After removing the supernatant, the cell pellet was frozen in liquid nitrogen and was treated
503 with 150 µL of 1.85 M NaOH–7.4% 2-mercaptoethanol for 15 min on ice. Then, 150 µL of 50% TCA
504 was added to the cell suspension to precipitate proteins on ice for 10 min. After removing the supernatant,
505 the proteins were washed twice with acetone and were denatured with the sample buffer at 95 °C for 5
506 min. Proteins were separated by SDS-PAGE and transferred to Immobilon PVDF membranes (EMD
507 Millipore, Billerica, MA, USA). The membrane was incubated for 1 h with antibodies. The following
508 antibodies were used: a monoclonal antibody for HA (Medical & Biological Laboratories Co. Ltd.,

509 Nagoya, Japan), a rabbit polyclonal antibody for Adh1 (Rockland Immunochemicals, Inc., Gilbersville,
510 PA, USA), a rabbit polyclonal antibody for Pma1 (Usami *et al.*, 2014), a mouse monoclonal antibody
511 for Slt2 (cat. no. sc-133189, Santa Cruz Biotechnology, TX, USA), a rabbit monoclonal antibody
512 phospho-p44/42 MAPK (Erk1/2, Thr202/Tyr204; cat no. 4376, Cell Signaling Technology, MA, USA)
513 to detect phospho-Slt2, a rabbit polyclonal antibody for Ypk1 (a kind gift from Dr. Mitsuaki Tabuchi of
514 Kagawa University), and a rabbit monoclonal antibody for Phospho-PKC (pan) (zeta Thr410) (190D10)
515 (cat. no. 2060, Signaling Technology) to detect phospho-Ypk1. The membranes were washed and
516 incubated for 30 min with horseradish peroxidase-conjugated goat anti-rabbit IgG (GE Healthcare Bio-
517 Sciences, NJ, USA). Labeling was performed using an enhanced chemiluminescence (ECL) select kit
518 (GE Healthcare Bio-Sciences). The chemiluminescence signals were detected in an ImageQuant
519 LAS4000 mini (GE Healthcare Life Sciences, NJ, USA)
520
521 **Image collection and analyses on confocal laser microscope**
522 Cells expressing GFP- or mCherry-tagged proteins were imaged using a confocal laser microscope (FV-
523 3000) equipped with an objective lens UPLAPO60XOHR (NA 1.5) (Olympus, Co. Ltd., Tokyo, Japan).
524 To determine the cell volume, cells were assumed to be spheres or ellipsoids. Using Tat1-GFP as a cell
525 membrane marker (Ishii *et al.*, 2022), cross-sectional images of > 100 cells cultured under each
526 condition were acquired. CellSens software (Olympus, Co. Ltd) was used to mark Tat1-GFP as a circle
527 or ellipse, and the radius (r μm) or long (a μm) and short radii (b μm) were calculated. For spheres, the
528 volume (μm^3) was approximated by $V = 4/3\pi * r^3$, and for ellipsoids, $V = 4/3\pi * a * b^2$. Changes in cell
529 volume due to high-pressure incubation were measured by acquiring images at 0.1 MPa, immediately
530 after depressurization. Colocalization of Lsp1-mCherry with Slm1-GFP or Avo3-3×mCherry with Slm1-
531 GFP was analyzed in more than 50 cells from three independent experiments using cellSens software
532 and represented by the Pearson colocalization coefficient. An IX70 epifluorescence inverted microscope
533 (Olympus, Co. Ltd.) was used for imaging.
534
535 **Determination of glycerol concentration**
536 Culture medium containing cells of 1.0 OD_{600} (1.65×10^7 cells) was centrifuged at 6,000 × g for 1 min
537 to separate the supernatant and cell pellet. The cell pellet was dissolved in 100 μL of sterilized deionized
538 water and the mixture was heated at 95 °C for 10 min. After cooling to room temperature, the mixture

539 was centrifuged at 21,500 × *g* for 10 min to collect the supernatant. Glycerol concentrations in the
540 samples were determined using a glycerol colorimetric assay kit (item no. 10010755, Cayman Chemical
541 Company, MI, USA) with an appropriate dilution.
542
543 **Measurement of osmotic pressure**
544 The osmotic pressure of SC medium was measured using a Fiske 210 osmometer (Advanced
545 Instruments, MA, USA).
546
547 **Transmission electron microscopy observation**
548 Samples for TEM observation were prepared as described previously (Yamaguchi *et al.*, 2021a;
549 Yamaguchi *et al.*, 2021b), with modifications. Cells cultured at 0.1 MPa or 25 MPa for 24 h in the SC
550 medium were briefly centrifuged at 760 × *g* following depressurization, and less than 1 μL of the cell
551 suspension was sandwiched between two copper disks (3 mm diameter) that had been prehydrophilized.
552 The copper disks were then sandwiched between reverse-acting tweezers and dropped into a coolant for
553 quick freezing. An isopentane : ethanol (4 : 1) mixture cooled with liquid nitrogen to a sherbet-like
554 consistency (approximately -130 °C) was used as the coolant. The copper disks were immediately
555 transferred to liquid nitrogen, cracked open, and then transferred to a fixing solution cooled with liquid
556 nitrogen. Ethanol containing 2% glutaraldehyde and 1% tannic acid was used as a fixing solution. The
557 samples in the fixing solution were kept at -80 °C for 48 h, -20 °C for 2 h, 4 °C for 2 h, and finally
558 returned to room temperature, in that order. Cells on copper disks were immersed in dehydrated ethanol
559 for 30 min thrice and then overnight. Propylene oxide : resin (Agar low viscosity resin LV, cat. no.
560 R1078, Agar Scientific Ltd, Essex, UK) mixture was used for resin replacement of the samples, with the
561 following mixing ratios in sequence; 1 : 0 (30 min, twice), 2 : 1 (1 h, once), 1 : 2 (1 h, once), 0 : 1
562 (overnight, once). The resin-substituted samples were allowed to solidify for 24 h at 60 °C. Ultrathin
563 sections of 70 nm thickness were then prepared using an Ultracut E ultramicrotome (Reichert-Jung,
564 Austria). The sections were stained with EM Stainer (cat no. 336, Nissin EM, Tokyo, Japan) for 30 min
565 and lead stain (Sigma-Aldrich, MO, USA) for 30 min. The samples were observed using a transmission
566 electron microscope JEM-2100 (JEOL, Tokyo, Japan) equipped with a thermionic electron emission
567 electron gun (LaB6 filament) at an acceleration voltage of 100 kV.
568

Acknowledgments

We would like to thank Drs. Satoshi Yoshida, Jiro Toshima, Makoto Nagano, and Takuma Kishimoto for providing plasmids; Drs. David Levin and Hidetoshi Iida for providing yeast strains; Dr. Mitsuaki Tabuchi for providing the rabbit polyclonal antibody for Ypk1 and for his critical reading of this manuscript; Mrs. Katsuyuki Uematsu and Yosuke Ishihara for technical assistances on TEM sample preparations; and the laboratory members for facilitating valuable discussions. TEM observation was supported by Center for Instrumental Analysis, College of Science and Engineering, Aoyama Gakuin University.

Funding

This work was supported by a grant from the Japan Society for the Promotion of Science (No. 18K05397 and 22H02247 to F. Abe) and a fund from Aoyama Gakuin University (Aoyama Vision 2019–2021).

Author contributions

Takahiro Mochizuki: Conceptualization and investigation; Toshiki Tanigawa: Conceptualization and investigation; Seiya Shindo: Investigation; Momoka Suematsu: Investigation; Yuki Oguchi: Investigation; Tetsuo Mioka: Cooperation; Yusuke Kato: Cooperation; Mina Fujiyama: Investigation; Eri Hatano: Investigation; Masashi Yamaguchi: Cooperation; Hiroji Chibana: Cooperation; Fumiyoshi Abe: Conceptualization, supervision, writing – original draft, and review and editing.

Competing interests

The authors declare no competing interests.

References

Abe, F. (2021). Molecular responses to high hydrostatic pressure in eukaryotes: Genetic insights from studies on *Saccharomyces cerevisiae*. Biology (Basel) *10*, 10.3390/biology10121305.

Abe, F. (2007). Induction of *DAN/TIR* yeast cell wall mannoprotein genes in response to high hydrostatic pressure and low temperature. FEBS Lett. *581*, 4993-4998.

Abe, F., and Horikoshi, K. (2000). Tryptophan permease gene *TAT2* confers high-pressure growth in

600 *Saccharomyces cerevisiae*. Mol. Cell. Biol. *20*, 8093-8102.
601 Abe, F., and Iida, H. (2003). Pressure-induced differential regulation of the two tryptophan permeases
602 Tat1 and Tat2 by ubiquitin ligase Rsp5 and its binding proteins, Bul1 and Bul2. Mol. Cell. Biol. *23*,
603 7566-7584.
604 Abe, F., Kato, C., and Horikoshi, K. (1999). Pressure-regulated metabolism in microorganisms. Trends
605 Microbiol. *7*, 447-453.
606 Abe, F., and Minegishi, H. (2008). Global screening of genes essential for growth in high-pressure and
607 cold environments: Searching for basic adaptive strategies using a yeast deletion library. Genetics
608 *178*, 851-872.
609 Abramova, N. E., Cohen, B. D., Sertil, O., Kapoor, R., Davies, K. J., and Lowry, C. V. (2001).
610 Regulatory mechanisms controlling expression of the *DAN/TIR* mannoprotein genes during
611 anaerobic remodeling of the cell wall in *Saccharomyces cerevisiae*. Genetics *157*, 1169-1177.
612 Afoke, N. Y., Byers, P. D., and Hutton, W. C. (1987). Contact pressures in the human hip joint. J. Bone
613 Joint Surg. Br. *69*, 536-541.
614 Ahmadpour, D., Maciaszczyk-Dziubinska, E., Babazadeh, R., Dahal, S., Migocka, M., Andersson, M.,
615 Wysocki, R., Tamas, M. J., and Hohmann, S. (2016). The mitogen-activated protein kinase Slt2
616 modulates arsenite transport through the aquaglyceroporin Fps1. FEBS Lett. *590*, 3649-3659.
617 Atilgan, E., Magidson, V., Khodjakov, A., and Chang, F. (2015). Morphogenesis of the fission yeast cell
618 through cell wall expansion. Curr. Biol. *25*, 2150-2157.
619 Babst, M. (2019). Eisosomes at the intersection of TORC1 and TORC2 regulation. Traffic *20*, 543-551.
620 Banavar, S. P., Gomez, C., Trogdon, M., Petzold, L. R., Yi, T. M., and Campas, O. (2018). Mechanical
621 feedback coordinates cell wall expansion and assembly in yeast mating morphogenesis. PLoS
622 Comput. Biol. *14*, e1005940.
623 Beese, S. E., Negishi, T., and Levin, D. E. (2009). Identification of positive regulators of the yeast fps1
624 glycerol channel. PLoS Genet. *5*, e1000738.
625 Berchtold, D., Piccolis, M., Chiaruttini, N., Riezman, I., Riezman, H., Roux, A., Walther, T. C., and
626 Loewith, R. (2012). Plasma membrane stress induces relocalization of slm proteins and activation
627 of TORC2 to promote sphingolipid synthesis. Nat. Cell Biol. *14*, 542-547.
628 Bi, E., and Park, H. O. (2012). Cell polarization and cytokinesis in budding yeast. Genetics *191*, 347-
629 387.
630 Blomberg, A. (2022). Yeast osmoregulation - glycerol still in pole position. FEMS Yeast Res. *22*,
631 10.1093/femsyr/foac035.
632 Bourges, A. C., Torres Montaguth, O. E., Ghosh, A., Tadesse, W. M., Declerck, N., Aertsen, A., and
633 Royer, C. A. (2017). High pressure activation of the mrr restriction endonuclease in escherichia
634 coli involves tetramer dissociation. Nucleic Acids Res. *45*, 5323-5332.
635 Brachmann, C. B., Davies, A., Cost, G. J., Caputo, E., Li, J., Hieter, P., and Boeke, J. D. (1998). Designer
636 deletion strains derived from *Saccharomyces cerevisiae* S288C: A useful set of strains and plasmids

637 for PCR-mediated gene disruption and other applications. Yeast *14*, 115-132.
638 Chen, B., Hoffmann, R., and Cammi, R. (2017). The effect of pressure on organic reactions in fluids-a
639 new theoretical perspective. Angew. Chem. Int. Ed Engl. *56*, 11126-11142.
640 Cruz, S., Munoz, S., Manjon, E., Garcia, P., and Sanchez, Y. (2013). The fission yeast cell wall stress
641 sensor-like proteins Mtl2 and Wsc1 act by turning on the GTPase Rho1p but act independently of
642 the cell wall integrity pathway. Microbiologyopen *2*, 778-794.
643 Davi, V., Chevalier, L., Guo, H., Tanimoto, H., Barrett, K., Couturier, E., Boudaoud, A., and Minc, N.
644 (2019). Systematic mapping of cell wall mechanics in the regulation of cell morphogenesis. Proc.
645 Natl. Acad. Sci. U. S. A. *116*, 13833-13838.
646 de Nadal, E., and Posas, F. (2022). The HOG pathway and the regulation of osmoadaptive responses in
647 yeast. FEMS Yeast Res. *22*, 10.1093/femsyr/foac013.
648 Domitrovic, T., Fernandes, C. M., Boy-Marcotte, E., and Kurtenbach, E. (2006). High hydrostatic
649 pressure activates gene expression through Msn2/4 stress transcription factors which are involved
650 in the acquired tolerance by mild pressure precondition in *Saccharomyces cerevisiae*. FEBS Lett.
651 *580*, 6033-6038.
652 Douglas, L. M., and Konopka, J. B. (2014). Fungal membrane organization: The eisosome concept.
653 Annu. Rev. Microbiol. *68*, 377-393.
654 Dupres, V., Alsteens, D., Wilk, S., Hansen, B., Heinisch, J. J., and Dufrene, Y. F. (2009). The yeast Wsc1
655 cell surface sensor behaves like a nanospring in vivo. Nat. Chem. Biol. *5*, 857-862.
656 Elhasi, T., and Blomberg, A. (2019). Integrins in disguise - mechanosensors in *Saccharomyces*
657 *cerevisiae* as functional integrin analogues. Microb. Cell. *6*, 335-355.
658 Eltschinger, S., and Loewith, R. (2016). TOR complexes and the maintenance of cellular homeostasis.
659 Trends Cell Biol. *26*, 148-159.
660 Funada, C., Tanino, N., Fukaya, M., Mikajiri, Y., Nishiguchi, M., Otake, M., Nakasuji, H., Kawahito,
661 R., and Abe, F. (2022). SOD1 mutations cause hypersensitivity to high-pressure-induced oxidative
662 stress in *Saccharomyces cerevisiae*. Biochim. Biophys. Acta Gen. Subj. *1866*, 130049.
663 Gietz, R. D., and Sugino, A. (1988). New yeast-*Escherichia coli* shuttle vectors constructed with in vitro
664 mutagenized yeast genes lacking six-base pair restriction sites. Gene *74*, 527-534.
665 Gonzalez-Rubio, G., Sastre-Vergara, L., Molina, M., Martin, H., and Fernandez-Acero, T. (2022).
666 Substrates of the MAPK Slt2: Shaping yeast cell integrity. J. Fungi (Basel) *8*, 368. doi:
667 10.3390/jof8040368.
668 Gualtieri, T., Ragni, E., Mizzi, L., Fascio, U., and Popolo, L. (2004). The cell wall sensor Wsc1p is
669 involved in reorganization of actin cytoskeleton in response to hypo-osmotic shock in
670 *Saccharomyces cerevisiae*. Yeast *21*, 1107-1120.
671 Heinisch, J. J., Dupres, V., Wilk, S., Jendretzki, A., and Dufrene, Y. F. (2010). Single-molecule atomic
672 force microscopy reveals clustering of the yeast plasma-membrane sensor Wsc1. PLoS One *5*,
673 e11104.

674 Hodder, E., Guppy, F., Covill, D., and Bush, P. (2020). The effect of hydrostatic pressure on proteoglycan
675 production in articular cartilage in vitro: A meta-analysis. Osteoarthritis Cartilage *28*, 1007-1019.
676 Hodge, W. A., Carlson, K. L., Fijan, R. S., Burgess, R. G., Riley, P. O., Harris, W. H., and Mann, R. W.
677 (1989). Contact pressures from an instrumented hip endoprosthesis. J. Bone Joint Surg. Am. *71*,
678 1378-1386.
679 Hohmann, S. (2002). Osmotic stress signaling and osmoadaptation in yeasts. Microbiol. Mol. Biol. Rev.
680 *66*, 300-372.
681 Ishii, R., Fukui, A., Sakihama, Y., Kitsukawa, S., Futami, A., Mochizuki, T., Nagano, M., Toshima, J.,
682 and Abe, F. (2022). Substrate-induced differential degradation and partitioning of the two
683 tryptophan permeases Tat1 and Tat2 into eisosomes in *Saccharomyces cerevisiae*. Biochim.
684 Biophys. Acta Biomembr. *1864*, 183858.
685 Iwahashi, H. (2015). Pressure-dependent gene activation in yeast cells. Subcell. Biochem. *72*, 407-422.
686 Jimenez-Gutierrez, E., Alegria-Carrasco, E., Sellers-Moya, A., Molina, M., and Martin, H. (2020). Not
687 just the wall: The other ways to turn the yeast CWI pathway on. Int. Microbiol. *23*, 107-119.
688 Kamada, Y., Fujioka, Y., Suzuki, N. N., Inagaki, F., Wullschleger, S., Loewith, R., Hall, M. N., and
689 Ohsumi, Y. (2005). Tor2 directly phosphorylates the AGC kinase Ypk2 to regulate actin polarization.
690 Mol. Cell. Biol. *25*, 7239-7248.
691 Kawada, D., Kobayashi, H., Tomita, T., Nakata, E., Nagano, M., Siekhaus, D. E., Toshima, J. Y., and
692 Toshima, J. (2015). The yeast Arf-GAP Glo3p is required for the endocytic recycling of cell surface
693 proteins. Biochim. Biophys. Acta *1853*, 144-156.
694 Kechagia, J. Z., Ivaska, J., and Roca-Cusachs, P. (2019). Integrins as biomechanical sensors of the
695 microenvironment. Nat. Rev. Mol. Cell Biol. *20*, 457-473.
696 Kim, K. Y., Truman, A. W., Caesar, S., Schlenstedt, G., and Levin, D. E. (2010). Yeast Mpk1 cell wall
697 integrity mitogen-activated protein kinase regulates nucleocytoplasmic shuttling of the Swi6
698 transcriptional regulator. Mol. Biol. Cell *21*, 1609-1619.
699 Kishimoto, T., Mioka, T., Itoh, E., Williams, D. E., Andersen, R. J., and Tanaka, K. (2021). Phospholipid
700 flippases and Sfk1 are essential for the retention of ergosterol in the plasma membrane. Mol. Biol.
701 Cell *32*, 1374-1392.
702 Kock, C., Arlt, H., Ungermann, C., and Heinisch, J. J. (2016). Yeast cell wall integrity sensors form
703 specific plasma membrane microdomains important for signaling. Cell. Microbiol. *18*, 1251-1267.
704 Kock, C., Dufrene, Y. F., and Heinisch, J. J. (2015). Up against the wall: Is yeast cell wall integrity
705 ensured by mechanosensing in plasma membrane microdomains? Appl. Environ. Microbiol. *81*,
706 806-811.
707 Kurosaka, G., Uemura, S., Mochizuki, T. *et al.* (2019). A novel ER membrane protein Ehg1/May24
708 plays a critical role in maintaining multiple nutrient permeases in yeast under high-pressure
709 perturbation. Sci. Rep. *9*, 18341-019-54925-1.
710 Ladoux, B., and Mege, R. M. (2017). Mechanobiology of collective cell behaviors. Nat. Rev. Mol. Cell

711 Biol. *18*, 743-757.
712 Laize, V., Gobin, R., Rousselet, G., Badier, C., Hohmann, S., Ripoche, P., and Tacnet, F. (1999).
713 Molecular and functional study of AQY1 from *Saccharomyces cerevisiae*: Role of the C-terminal
714 domain. Biochem. Biophys. Res. Commun. *257*, 139-144.
715 Lanze, C. E., Gandra, R. M., Foderaro, J. E., Swenson, K. A., Douglas, L. M., and Konopka, J. B. (2020).
716 Plasma membrane MCC/Eisosome domains promote stress resistance in fungi. Microbiol. Mol.
717 Biol. Rev. *84*, 10.1128/MMBR.00063-19. Print 2020 Nov 18.
718 Laz, E. V., Lee, J., and Levin, D. E. (2020). Crosstalk between *Saccharomyces cerevisiae* SAPKs Hog1
719 and Mpk1 is mediated by glycerol accumulation. Fungal Biol. *124*, 361-367.
720 Lee, J., Reiter, W., Dohnal, I., Gregori, C., Beese-Sims, S., Kuchler, K., Ammerer, G., and Levin, D. E.
721 (2013). MAPK Hog1 closes the S. cerevisiae glycerol channel Fps1 by phosphorylating and
722 displacing its positive regulators. Genes Dev. *27*, 2590-2601.
723 Lesage, G., and Bussey, H. (2006). Cell wall assembly in *Saccharomyces cerevisiae*. Microbiol. Mol.
724 Biol. Rev. *70*, 317-343.
725 Leskoske, K. L., Roelants, F. M., Martinez Marshall, M. N., Hill, J. M., and Thorner, J. (2017). The
726 stress-sensing TORC2 complex activates yeast AGC-family protein kinase Ypk1 at multiple novel
727 sites. Genetics *207*, 179-195.
728 Levin, D. E. (2011). Regulation of cell wall biogenesis in *Saccharomyces cerevisiae*: The cell wall
729 integrity signaling pathway. Genetics *189*, 1145-1175.
730 Levin, D. E. (2005). Cell wall integrity signaling in *Saccharomyces cerevisiae*. Microbiol. Mol. Biol.
731 Rev. *69*, 262-291.
732 Levin, D. E., and Bartlett-Heubusch, E. (1992). Mutants in the *S. cerevisiae PKC1* gene display a cell
733 cycle-specific osmotic stability defect. J. Cell Biol. *116*, 1221-1229.
734 Luyten, K., Albertyn, J., Skibbe, W. F., Prior, B. A., Ramos, J., Thevelein, J. M., and Hohmann, S. (1995).
735 Fps1, a yeast member of the MIP family of channel proteins, is a facilitator for glycerol uptake and
736 efflux and is inactive under osmotic stress. Embo j. *14*, 1360-1371.
737 Ma, H., Snook, L. A., Kaminskyj, S. G. W., and Dahms, T. E. S. (2005). Surface ultrastructure and
738 elasticity in growing tips and mature regions of aspergillus hyphae describe wall maturation.
739 Microbiology (Reading) *151*, 3679-3688.
740 Madden, K., and Snyder, M. (1998). Cell polarity and morphogenesis in budding yeast. Annu. Rev.
741 Microbiol. *52*, 687-744.
742 Martin, H., Rodriguez-Pachon, J. M., Ruiz, C., Nombela, C., and Molina, M. (2000). Regulatory
743 mechanisms for modulation of signaling through the cell integrity Slt2-mediated pathway in
744 *Saccharomyces cerevisiae*. J. Biol. Chem. *275*, 1511-1519.
745 Matsuki, H., Goto, M., Tada, K., and Tamai, N. (2013). Thermotropic and barotropic phase behavior of
746 phosphatidylcholine bilayers. Int. J. Mol. Sci. *14*, 2282-2302.
747 Merchan, S., Bernal, D., Serrano, R., and Yenush, L. (2004). Response of the *Saccharomyces cerevisiae*

748 Mpk1 mitogen-activated protein kinase pathway to increases in internal turgor pressure caused by
749 loss of Ppz protein phosphatases. Eukaryot. Cell. *3*, 100-107.
750 Minc, N., Boudaoud, A., and Chang, F. (2014). Mechanical forces of fission yeast growth. Curr. Biol.
751 *24*, 1436.
752 Mishra, R., Minc, N., and Peter, M. (2022). Cells under pressure: How yeast cells respond to mechanical
753 forces. Trends Microbiol. *30*, 495-510.
754 Mollapour, M., and Piper, P. W. (2007). Hog1 mitogen-activated protein kinase phosphorylation targets
755 the yeast Fps1 aquaglyceroporin for endocytosis, thereby rendering cells resistant to acetic acid.
756 Mol. Cell. Biol. *27*, 6446-6456.
757 Mollapour, M., Shepherd, A., and Piper, P. W. (2009). Presence of the Fps1p aquaglyceroporin channel
758 is essential for Hog1p activation, but suppresses Slt2(Mpk1)p activation, with acetic acid stress of
759 yeast. Microbiology (Reading) *155*, 3304-3311.
760 Muir, A., Roelants, F. M., Timmons, G., Leskoske, K. L., and Thorner, J. (2015). Down-regulation of
761 TORC2-Ypk1 signaling promotes MAPK-independent survival under hyperosmotic stress. elife *4*,
762 10.7554/eLife.09336.
763 Neeli-Venkata, R., Diaz, C. M., Celador, R., Sanchez, Y., and Minc, N. (2021). Detection of surface
764 forces by the cell-wall mechanosensor Wsc1 in yeast. Dev. Cell. *56*, 2856-2870.e7.
765 Orlean, P. (2012). Architecture and biosynthesis of the *Saccharomyces cerevisiae* cell wall. Genetics
766 *192*, 775-818.
767 Pattappa, G., Zellner, J., Johnstone, B., Docheva, D., and Angele, P. (2019). Cells under pressure - the
768 relationship between hydrostatic pressure and mesenchymal stem cell chondrogenesis. Eur. Cell.
769 Mater. *37*, 360-381.
770 Peterson, J., Zheng, Y., Bender, L., Myers, A., Cerione, R., and Bender, A. (1994). Interactions between
771 the bud emergence proteins Bem1p and Bem2p and rho-type GTPases in yeast. J. Cell Biol. *127*,
772 1395-1406.
773 Philip, B., and Levin, D. E. (2001). Wsc1 and Mid2 are cell surface sensors for cell wall integrity
774 signaling that act through Rom2, a guanine nucleotide exchange factor for Rho1. Mol. Cell. Biol.
775 *21*, 271-280.
776 Piao, H. L., Machado, I. M., and Payne, G. S. (2007). NPFXD-mediated endocytosis is required for
777 polarity and function of a yeast cell wall stress sensor. Mol. Biol. Cell *18*, 57-65.
778 Pruyne, D., and Bretscher, A. (2000). Polarization of cell growth in yeast. I. establishment and
779 maintenance of polarity states. J. Cell. Sci. *113 (Pt 3)*, 365-375.
780 Riggi, M., Niewola-Staszkowska, K., Chiaruttini, N. *et al.* (2018). Decrease in plasma membrane
781 tension triggers PtdIns(4,5)P2 phase separation to inactivate TORC2. Nat. Cell Biol. *20*, 1043-1051.
782 Rispal, D., Eltschinger, S., Stahl, M. *et al.* (2015). Target of rapamycin complex 2 regulates actin
783 polarization and endocytosis via multiple pathways. J. Biol. Chem. *290*, 14963-14978.
784 Roelants, F. M., Baltz, A. G., Trott, A. E., Fereres, S., and Thorner, J. (2010). A protein kinase network

785 regulates the function of aminophospholipid flippases. Proc. Natl. Acad. Sci. U. S. A. *107*, 34-39.
786 Roelants, F. M., Breslow, D. K., Muir, A., Weissman, J. S., and Thorner, J. (2011). Protein kinase Ypk1
787 phosphorylates regulatory proteins Orm1 and Orm2 to control sphingolipid homeostasis in
788 *Saccharomyces cerevisiae*. Proc. Natl. Acad. Sci. U. S. A. *108*, 19222-19227.
789 Roelants, F. M., Torrance, P. D., Bezman, N., and Thorner, J. (2002). Pkh1 and Pkh2 differentially
790 phosphorylate and activate Ypk1 and Ykr2 and define protein kinase modules required for
791 maintenance of cell wall integrity. Mol. Biol. Cell *13*, 3005-3028.
792 Roelants, F. M., Torrance, P. D., and Thorner, J. (2004). Differential roles of PDK1- and PDK2-
793 phosphorylation sites in the yeast AGC kinases Ypk1, Pkc1 and Sch9. Microbiology (Reading) *150*,
794 3289-3304.
795 Sabir, F., Loureiro-Dias, M. C., Soveral, G., and Prista, C. (2017). Functional relevance of water and
796 glycerol channels in *Saccharomyces cerevisiae*. FEMS Microbiol. Lett. *364*,
797 10.1093/femsle/fnx080.
798 Sakata, K. T., Hashii, K., Yoshizawa, K., Tahara, Y. O., Yae, K., Tsuda, R., Tanaka, N., Maeda, T., Miyata,
799 M., and Tabuchi, M. (2022). Coordinated regulation of TORC2 signaling by MCC/eisosome-
800 associated proteins, Pil1 and tetraspan membrane proteins during the stress response. Mol.
801 Microbiol. *117*, 1227-1244.
802 Schaber, J., Adrover, M. A., Eriksson, E. *et al.* (2010). Biophysical properties of *Saccharomyces*
803 *cerevisiae* and their relationship with HOG pathway activation. Eur. Biophys. J. *39*, 1547-1556.
804 Schmidt, A., Bickle, M., Beck, T., and Hall, M. N. (1997). The yeast phosphatidylinositol kinase
805 homolog TOR2 activates RHO1 and RHO2 via the exchange factor ROM2. Cell *88*, 531-542.
806 Schmidt, A., Schmelzle, T., and Hall, M. N. (2002). The RHO1-GAPs SAC7, BEM2 and BAG7 control
807 distinct RHO1 functions in *Saccharomyces cerevisiae*. Mol. Microbiol. *45*, 1433-1441.
808 Schoppner, P., Lutz, A. P., Lutterbach, B. J., Bruckner, S., Essen, L. O., and Mosch, H. U. (2022).
809 Structure of the yeast cell wall integrity sensor Wsc1 reveals an essential role of surface-exposed
810 aromatic clusters. J. Fungi (Basel) *8*, 10.3390/jof8040379.
811 Sikorski, R. S., and Hieter, P. (1989). A system of shuttle vectors and yeast host strains designed for
812 efficient manipulation of DNA in *Saccharomyces cerevisiae*. Genetics *122*, 19-27.
813 Siliciano, P. G., and Tatchell, K. (1984). Transcription and regulatory signals at the mating type locus in
814 yeast. Cell *37*, 969-978.
815 Straede, A., and Heinisch, J. J. (2007). Functional analyses of the extra- and intracellular domains of the
816 yeast cell wall integrity sensors Mid2 and Wsc1. FEBS Lett. *581*, 4495-4500.
817 Suzuki, A., Mochizuki, T., Uemura, S., Hiraki, T., and Abe, F. (2013). Pressure-induced endocytic
818 degradation of the *Saccharomyces cerevisiae* low-affinity tryptophan permease Tat1 is mediated by
819 Rsp5 ubiquitin ligase and functionally redundant PPxY motif proteins. Eukaryot. Cell. *12*, 990-997.
820 Tabuchi, M., Audhya, A., Parsons, A. B., Boone, C., and Emr, S. D. (2006). The phosphatidylinositol
821 4,5-biphosphate and TORC2 binding proteins Slm1 and Slm2 function in sphingolipid regulation.

822 Mol. Cell. Biol. *26*, 5861-5875.
823 Tamas, M. J., Luyten, K., Sutherland, F. C. *et al.* (1999). Fps1p controls the accumulation and release
824 of the compatible solute glycerol in yeast osmoregulation. Mol. Microbiol. *31*, 1087-1104.
825 Thorsen, M., Di, Y., Tangemo, C. *et al.* (2006). The MAPK Hog1p modulates Fps1p-dependent arsenite
826 uptake and tolerance in yeast. Mol. Biol. Cell *17*, 4400-4410.
827 Uemura, S., Mochizuki, T., Amemiya, K., Kurosaka, G., Yazawa, M., Nakamoto, K., Ishikawa, Y., Izawa,
828 S., and Abe, F. (2020). Amino acid homeostatic control by TORC1 in *Saccharomyces cerevisiae*
829 under high hydrostatic pressure. J. Cell. Sci. *133*, 10.1242/jcs.245555.
830 Usami, Y., Uemura, S., Mochizuki, T., Morita, A., Shishido, F., Inokuchi, J., and Abe, F. (2014).
831 Functional mapping and implications of substrate specificity of the yeast high-affinity leucine
832 permease Bap2. Biochim. Biophys. Acta *1838*, 1719-1729.
833 Vay, H. A., Philip, B., and Levin, D. E. (2004). Mutational analysis of the cytoplasmic domain of the
834 Wsc1 cell wall stress sensor. Microbiology (Reading) *150*, 3281-3288.
835 Wilk, S., Wittland, J., Thywissen, A., Schmitz, H. P., and Heinisch, J. J. (2010). A block of endocytosis
836 of the yeast cell wall integrity sensors Wsc1 and Wsc2 results in reduced fitness *in vivo*. Mol. Genet.
837 Genomics *284*, 217-229.
838 Winter, R. (2002). Synchrotron X-ray and neutron small-angle scattering of lyotropic lipid mesophases,
839 model biomembranes and proteins in solution at high pressure. Biochim. Biophys. Acta *1595*, 160-
840 184.
841 Winzeler, E. A., Shoemaker, D. D., Astromoff, A. *et al.* (1999). Functional characterization of the *S.*
842 *cerevisiae* genome by gene deletion and parallel analysis. Science *285*, 901-906.
843 Yamaguchi, M., Taguchi, M., Uematsu, K., Takahashi-Nakaguchi, A., Sato-Okamoto, M., and Chibana,
844 H. (2021a). Sandwich freezing device for rapid freezing of viruses, bacteria, yeast, cultured cells
845 and animal and human tissues in electron microscopy. Microscopy (Oxf) *70*, 215-223.
846 Yamaguchi, M., Takahashi-Nakaguchi, A., Uematsu, K., Taguchi, M., Sato-Okamoto, M., and Chibana,
847 H. (2021b). Rapid freezing using sandwich freezing device for good ultrastructural preservation of
848 biological specimens in electron microscopy. J. Vis. Exp. *(173). doi*, 10.3791/62431.
849 Yoshida, S., Bartolini, S., and Pellman, D. (2009). Mechanisms for concentrating Rho1 during
850 cytokinesis. Genes Dev. *23*, 810-823.
851 Yoshino, D., Funamoto, K., Sato, K., Kenry, Sato, M., and Lim, C. T. (2020). Hydrostatic pressure
852 promotes endothelial tube formation through aquaporin 1 and Ras-ERK signaling. Commun. Biol.
853 *3*, 152-020-0881-9.
854
855

Table 1. Strains used in this study

Strain	Genotype	Source or reference
BY4742	*MATα his3*Δ1 *leu2Δ*0 *lys2*Δ0 *ura3*Δ0	(Brachmann *et al.*, 1998)
16672	*wsc1*Δ::*kanMX4* in BY4742	(Winzeler *et al.*, 1999)
11161	*wsc2*Δ::*kanMX4* in BY4742	(Winzeler *et al.*, 1999)
16255	*wsc3*Δ::*kanMX4* in BY4742	(Winzeler *et al.*, 1999)
15241	*mid2*Δ::*kanMX4* in BY4742	(Winzeler *et al.*, 1999)
14653	*mtl1*Δ::*kanMX4* in BY4742	(Winzeler *et al.*, 1999)
14700	*rom1*Δ::*kanMX4* in BY4742	(Winzeler *et al.*, 1999)
15280	*rom2*Δ::*kanMX4* in BY4742	(Winzeler *et al.*, 1999)
16152	*bem2*Δ::*kanMX4* in BY4742	(Winzeler *et al.*, 1999)
14225	*sac7*Δ::*kanMX4* in BY4742	(Winzeler *et al.*, 1999)
13937	*lrg1*Δ::*kanMX4* in BY4742	(Winzeler *et al.*, 1999)
12390	*bag7*Δ::*kanMX4* in BY4742	(Winzeler *et al.*, 1999)
DL100	*MAT*a *his4 leu2-3,112 trp1-1 ura3-52 can1*	(Siliciano and Tatchell, 1984)
DL376	*pkc1*Δ::*Leu2* in DL100	(Levin and Bartlett-Heubusch, 1992)
11328	*bck1*Δ::*kanMX4* in BY4742	(Winzeler *et al.*, 1999)
12487	*mkk1*Δ::*kanMX4* in BY4742	(Winzeler *et al.*, 1999)
12112	*mkk2*Δ::*kanMX4* in BY4742	(Winzeler *et al.*, 1999)
10993	*slt2*Δ::*kanMX4* in BY4742	(Winzeler *et al.*, 1999)
TMY1482	*SWI4-GFP*::*HIS3* in BY4742	This study
12739	*rlm1*Δ::*kanMX4* in BY4742	(Winzeler *et al.*, 1999)
16109	*swi4*Δ::*kanMX4* in BY4742	(Winzeler *et al.*, 1999)
14131	*swi6*Δ::*kanMX4* in BY4742	(Winzeler *et al.*, 1999)
AFY7	*PIL1*-mCherry::*URA3* in BY4742	(Ishii *et al.*, 2022)
MSY1	*NCE102*-mCherry::*URA3* in BY4742	This study
MSY17	*SUR7*-mCherry::*URA3* in BY4742	This study
11531	*fps1*Δ::*kanMX4* in BY4742	(Winzeler *et al.*, 1999)
11446	*gpp1*Δ::*kanMX4* in BY4742	(Winzeler *et al.*, 1999)
10199	*gpp2*Δ::*kanMX4* in BY4742	(Winzeler *et al.*, 1999)
13718	*gpd1*Δ::*kanMX4* in BY4742	(Winzeler *et al.*, 1999)
11751	*gpd2*Δ::*kanMX4* in BY4742	(Winzeler *et al.*, 1999)
TTY146	*fps1*Δ::*HphMX6 gpp1*::*kanMX4* in BY4742	This study
TTY147	*fps1*Δ*::HphMX6 gpd1*::*kanMX4* in BY4742	This study
TTY108	*SLM1-GFP*::*HIS3 LSP1-mCherry*::*URA3* in BY4742	This study
TTY113	*SLM1-GFP::HIS3 AVO3-3×mCherry*::*URA3* in BY4742	This study
14976	*ypk1*Δ::*kanMX4* in BY4742	(Winzeler *et al.*, 1999)

Table 2. Plasmids used in this study

Plasmid	Description	Source or reference
pUA35	3HA *URA3 CEN*4	Laboratory stock
pTM35	*GFP URA3 CEN*4	Laboratory stock
YEplac181	*LEU2 2 μ*	(Gietz and Sugino, 1988)
YCplac22	*TRP1 CEN4*	(Gietz and Sugino, 1988)
pRS313	*HIS3 CEN6*	(Sikorski and Hieter, 1989)
pTAT1-GFP	*TAT1*-GFP driven by its own promoter in pRS313	This study
pMB1	*WSC1*-3HA driven by its own promoter in pUA35	This study
pMB23	*WSC1*-3HA-Y303A driven by its own promoter in pUA35	This study
pMB74	*WSC1*-3HA-N344A-P345A-F346A driven by its own promoter in pUA35	This study
pSS21	*WSC1*-GFP driven by its own promoter in pTM35	This study
pMB80	*WSC1*-3HA-N344A-P345A-F346A driven by its own promoter in pTM35	This study
SP333	HA-*RHO1* driven by its own promoter *LEU2 CEN*	(Yoshida *et al.*, 2009)
SP335	HA-*RHO1*-F35L driven by its own promoter *LEU2 CEN*	(Yoshida *et al.*, 2009)
SP336	HA-*RHO1*-Q68H driven by its own promoter *LEU2 CEN*	(Yoshida *et al.*, 2009)
pME29	*PKC1* driven by its own promoter in YEplac181	This study
pME30	*PKC1*-R398P driven by its own promoter in YEplac181	This study
pTNK5	*FPS1* driven by its own promoter in pUA35	This study
pTNK8	*FPS1*-T231A driven by its own promoter in pUA35	This study
pTNK9	*FPS1*-S537A driven by its own promoter in pUA35	This study
pTNK10	*FPS1*-S570A driven by its own promoter in pUA35	This study
pTNK22	*FPS1*-S181A-S185A driven by its own promoter in pUA35	This study
pTNK23	*FPS1*-S181A-S185A-S570A driven by its own promoter in pUA35	This study
pSS10	*FPS1*-3HA driven by its own promoter in pUA35	This study
pSS26	*FPS1*-3HA-S537A driven by its own promoter in pUA35	This study
pSS12	*FPS1*-3HA-S570A driven by its own promoter in pUA35	This study
pSS16	*FPS1*-3HA-S181A-S185A driven by its own promoter in pUA35	This study
pSS14	*FPS1*-3HA-S181A-S185A-S570A driven by its own promoter in pUA35	This study
pSS6	*YPK1* driven by its own promoter in pUA35	This study
pTNK11	*YPK1*-S51A-S71A driven by its own promoter in pUA35	This study
pTNK7	*YPK1*-T504A driven by its own promoter in pUA35	This study
pTNK14	*YPK1*-S644A-T662A driven by its own promoter in pUA35	This study
pTM102	pBSK (+) -*SFK1*-3×mCherry	(Kishimoto *et al.*, 2021)
pJT6	GFP *HIS3*	(Kawada *et al.*, 2015)
pJT601	mCherry *URA3*	(Kawada *et al.*, 2015)

856

857 **Figure legends**

858 Fig. 1. Schematic representation of the CWI pathway in *Saccharomyces cerevisiae*. Five cell wall sensor
859 proteins are depicted. Upon cell wall stress, Wsc1 first clusters at the cell surface. Binding of the
860 GDP/GTP exchanging factor, Rom2, to the cytoplasmic tail of Wsc1 activates the small GTPase, Rho1.
861 Rho1-GTP activates the protein kinase C, Pkc1, which activates a conserved mitogen-activated protein
862 kinase (MAPK) cascade. The cascade consists of Bck1 (MAPKKK), Mkk1/Mkkk2 (MAPKKs), and
863 Slt2 (MAPK). Phosphorylated Slt2 translocates into the nucleus and promotes cell cycle progression
864 through the SBF complex and transcription of genes encoding cell wall proteins by Rlm1. Slt2 also
865 phosphorylates the aquaglyceroporin, Fps1, and promotes Fps1 opening to expel glycerol. When cells
866 are stressed, tension is applied to the plasma membrane, causing the loss of the eisosome, a plasma
867 membrane invaginating structure. Slm1/Slm2 localized in the eisosome migrate to TORC2.
868 Consequently, TORC2 is activated and phosphorylates Ypk1. Phosphorylated Ypk1 also phosphorylates
869 Fps1, positively regulating glycerol efflux. The phosphorylation sites, kinases, and functional motifs in
870 major proteins used in this study are outlined below. CRD (8C), cysteine-rich domain (C27, C49, C53,
871 C69, C71, C86, C90, and C98); STR, serine/threonine-rich domain (111–265 amino acid residues); NPF
872 motif, N344-P345-F346.

873

874 Fig. 2. Wsc1 is required for growth under high pressure. (A) Wild-type and mutant cells were cultured
875 in SC medium at 0.1 MPa or 25 MPa for 48 h with an initial OD_{600} = 0.01. Unless otherwise specified,
876 the high-pressure growth test was carried under this condition throughout the experiments. (B) Cells
877 with mutations in the extracellular domain of Wsc1 or the NPF>AAA substitution were cultured in SC
878 medium at 0.1 or 25 MPa. (C). Wild-type cells expressing Wsc1-GFP or the mutant forms were cultured
879 at 0.1 or 25 MPa for 3 h and were observed under a confocal laser microscope immediately after
880 depressurization. Data are presented as mean ± standard deviation of three independent experiments.

881

882 Fig. 3. CWI pathway is activated by high pressure. (A) Mutant strains with various defects in the CWI
883 pathway were cultured in SC medium at 0.1 or 25 MPa. (B) *rom2*Δ cells expressing Rho1 or Pck1
884 derivatives were cultured in SC medium at 0.1 or 25 MPa. (C) Mutant strains with various defects in
885 the CWI pathway were cultured in SC medium at 0.1 or 25 MPa. Strains DL100 and DL376 harboring
886 YCplac22 (*TRP1* and *CEN*) were used to examine the *PKC1* deficiency (left). (D) Wild-type cells were

887 cultured in SC medium under various pressure conditions for 3 h. Slt2 and phosphorylated Slt2 (P-Slt2)
888 were detected using western blotting using specific antibodies. The relative intensities, P-Slt2/Adh1 and
889 Slt2/Adh1, were quantified in an ImageQuant LAS4000 mini. (E) Wild-type or *wsc1*Δ cells were
890 cultured in SC medium at 0.1 or 25 MPa for 3 h. Western blotting was performed as in (D). Data are
891 presented as mean ± standard deviation of three independent experiments.
892
893 Fig. 4. High pressure promotes nuclear translocation of Swi4. (A) Wild-type cells expressing Swi4-GFP
894 were incubated with 15 μg/mL nocodazole for 2 h at 0.1 MPa. The cells were then cultured for another
895 5 h at 0.1 or 25 MPa and were observed after depressurization. The percentages of cells with Swi4-GFP
896 in the nucleus in more than 300 cells are shown. (B) Mutant strains were cultured in SC medium at 0.1
897 or 25 MPa. Data are presented as mean ± standard deviation of three independent experiments.
898
899 Fig. 5. High pressure causes cell swelling and loss of the eisosome structure. (A) Wild-type cells co-
900 expressing Tat1-GFP (plasma membrane marker) and Nce102-mCherry (eisosome marker) were
901 cultured in SC medium at 0.1, 25, or 50 MPa for 3 h. After depressurization, cells were observed at 0.1
902 MPa under a confocal laser microscope. Cross-section images are shown. (B) Cells co-expressing Tat1-
903 GFP and Nce102-mCherry, Pil1-mCherry, or Sur7-mCherry were cultured in SC medium at 0.1 or 25
904 MPa for 1 or 3 h. Pearson's correlation coefficient (PCC) was obtained for cell surface images from 63
905 cells in three independent experiments. (C) Changes in cell volume when cultured under high pressure.
906 Cells were cultured at 0.1, 25, or 50 MPa for 1 or 3 h in SC medium with or without 1 M sorbitol. The
907 cell volume was calculated from the cell diameter of more than 300 cells after depressurization in three
908 independent experiments.
909
910 Fig. 6. Glycerol efflux via Aquaglyceroporin Fps1 is required for high-pressure growth. (A) Wild-type
911 and *fps1*Δ cells were cultured in SC medium with or without 1 M sorbitol at 0.1 or 25 MPa. (B) Mutants
912 defective in glycerol synthesis were cultured in SC medium at 0.1 or 25 MPa. (C) Measurement of
913 intracellular and extracellular glycerol levels after incubating cells at 0.1 or 25 MPa for 24 h with an
914 initial OD_{600} = 0.1. Glycerol levels were quantified using a Glycerol assay kit. Data are presented as
915 mean ± standard deviation of three independent experiments.
916

917 Fig. 7. Ultrastructure of the cells observed using transmission electron microscopy. Wild-type and *fps1*Δ
918 cells were cultured at 0.1 or 25 MPa for 24 h, and after depressurization, the samples were subjected to
919 rapid freezing using the sandwich method. In *fps1*Δ cells, the points of cell wall breakage are indicated
920 by arrows. Scale bars, 1.0 μm
921
922 Fig. 8. Slt2-dependent phosphorylation of Fps1 is required for growth under high pressure. (A) The Fps1
923 phosphorylation-site mutants were cultured in SC medium at 0.1 or 25 MPa. (B) Electrophoretic
924 mobility of Fps1-3HA and its mutant forms was analyzed using western blotting. Cells were cultured at
925 0.1 or 25 MPa for 3 h, and whole cell extracts were prepared. The arrowhead indicates a higher-
926 molecular weight band of Phospho-Fps1 (P-Fps1). The relative intensities, P-Fps1/Pma1 at 0.1 and 25
927 MPa, were quantified in an ImageQuant LAS4000 mini. (C) Wild-type, *slt2*Δ, *hog1*Δ, *swi4*Δ, and *swi6*Δ
928 cells were cultured in SC medium with or without 1 M sorbitol at 0.1 or 25 MPa. (D) Wild-type cells
929 were cultured in SC medium with or without 1 M sorbitol at 0.1 or 25 MPa for 3 h. Western blotting
930 was performed as in Fig. 3D. (E) *slt2*Δ cells expressing Fps1, Fps1^{S537A} or Fps1^{S537E} were cultured in SC
931 medium at 0.1 or 25 MPa. (F) The Ypk1 phosphorylation-site mutants were cultured in SC medium at
932 0.1 or 25 MPa. (G) The Fps1 phosphorylation-site mutants were cultured in SC medium at 0.1 or 25
933 MPa. Data are presented as mean ± standard deviation of three independent experiments.
934
935 Fig. 9. Model depicting Wsc1-dependent high-pressure signaling pathway in yeast. When pressure is
936 applied to the cell, an excessive influx of water into the cell occurs. Perturbation of the cell wall by high
937 pressure causes further water influx, and the cell becomes at a risk of rupture. To prevent this, Wsc1
938 detects cell wall stretching and activates the CWI pathway. Once the CWI pathway is activated, Slt2
939 kinase phosphorylates the aquaglyceroporin Fps1. Phosphorylated Fps1 promotes its opening, which
940 allows cells to expel glycerol, adjusting the osmotic pressure balance across the plasma membrane.
941 TORC2-Ypk1 pathway is independent of the regulation of Fps1 under high pressure.
942
943 Fig. S1. TORC2-mediated Ypk1 phosphorylation by high pressure. (A) High pressure causes the
944 dissociation of a fraction of Slm1 from the eisosomes and its migration to TORC2. Wild-type cells co-
945 expressing Slm1-GFP and Lsp1-mCherry, or those co-expressing Slm1-GFP and Avo3-3×mCherry,
946 were cultured in SC medium at 0.1 or 25 MPa for 5 h. The cells were observed using confocal laser

947 microscopy immediately after depressurization. Colocalizations were analyzed in more than 50 cells
948 from three independent experiments using the cellSens software and represented by the PCC. (B) High
949 pressure promotes the phosphorylation level of Ypk1. Ypk1 and phosphorylated Ypk1 were detected
950 from whole cell extracts via western blotting, using antibodies for Ypk1 and phospho-PKC (pan) (zeta
951 Thr410) (190D10), respectively. The relative intensities, P-Ypk1/Adh1 and Ypk1/Adh1, were quantified
952 in an ImageQuant LAS4000 mini.
953
954

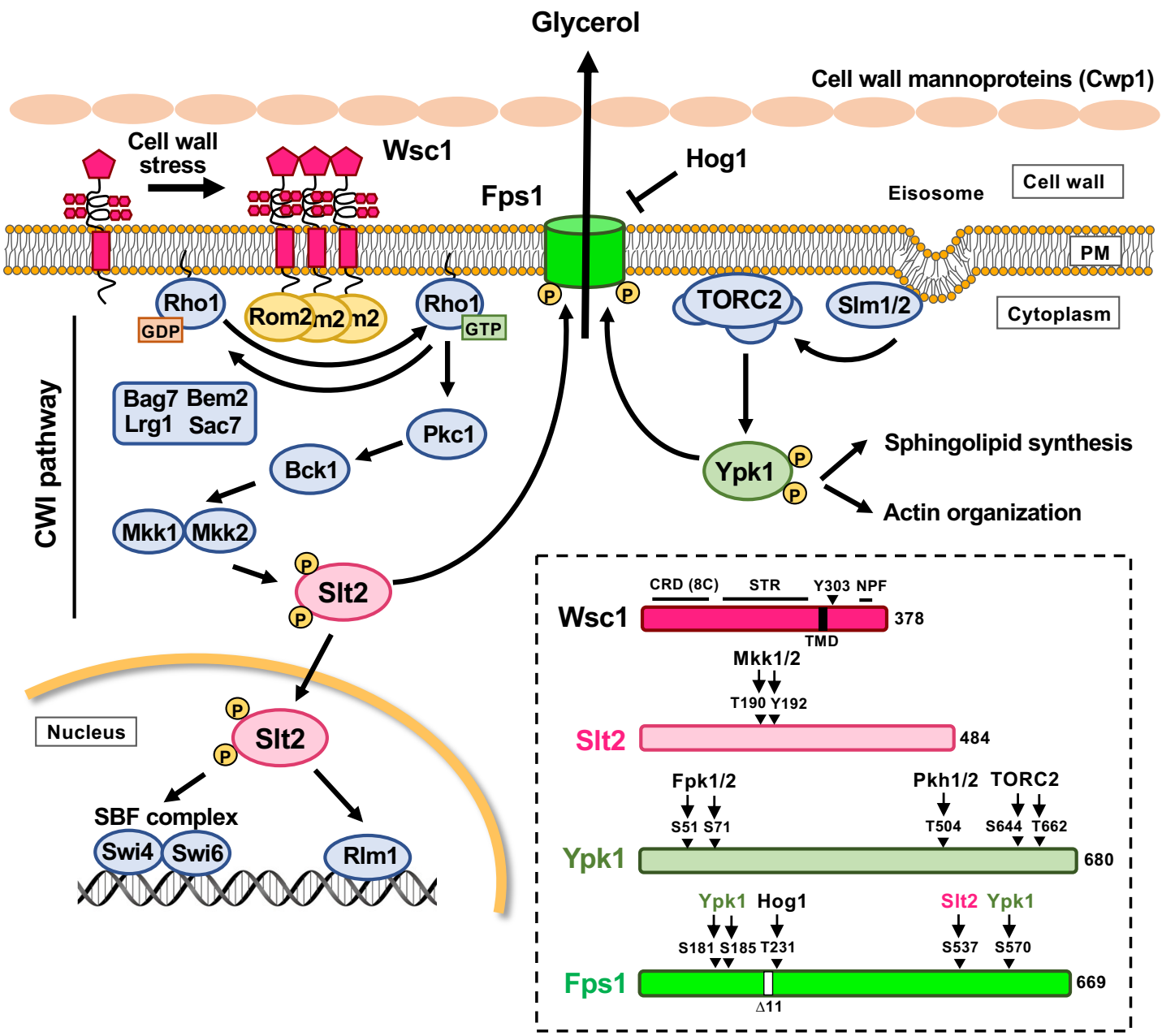

Fig. 1. Mochizuki *et al.*

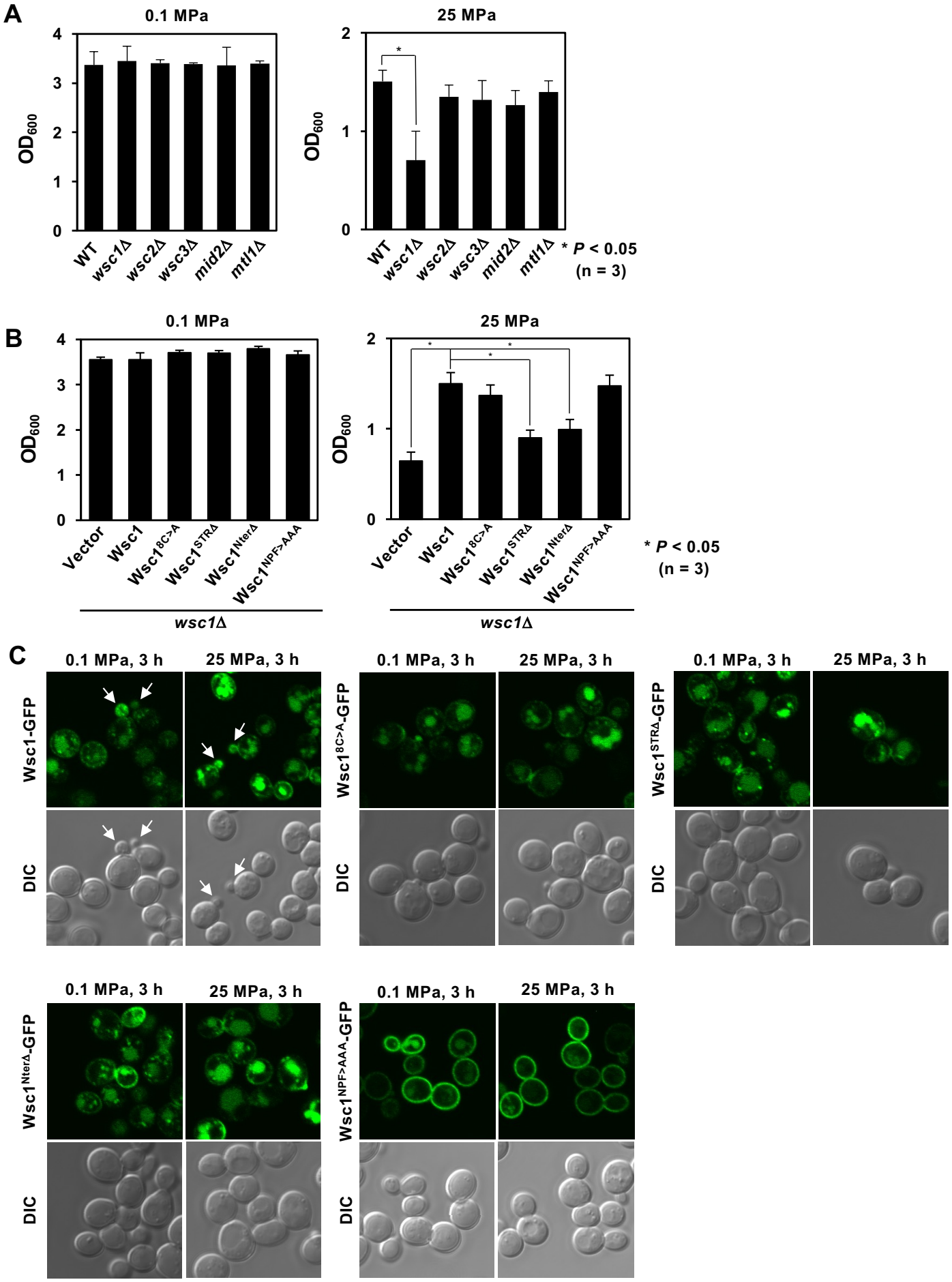

Fig. 2. Mochizuki *et al.*

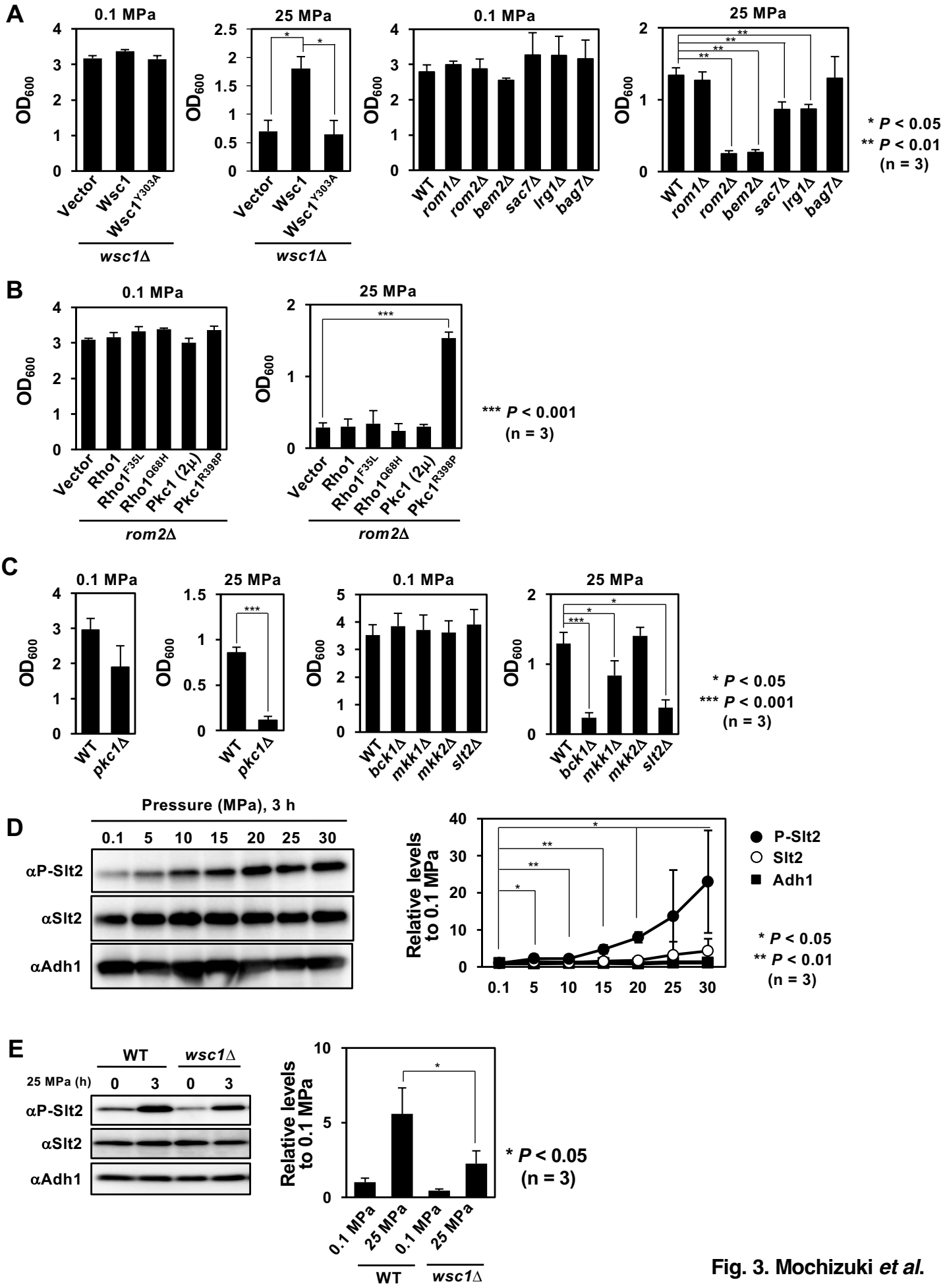

Fig. 3. Mochizuki *et al.*

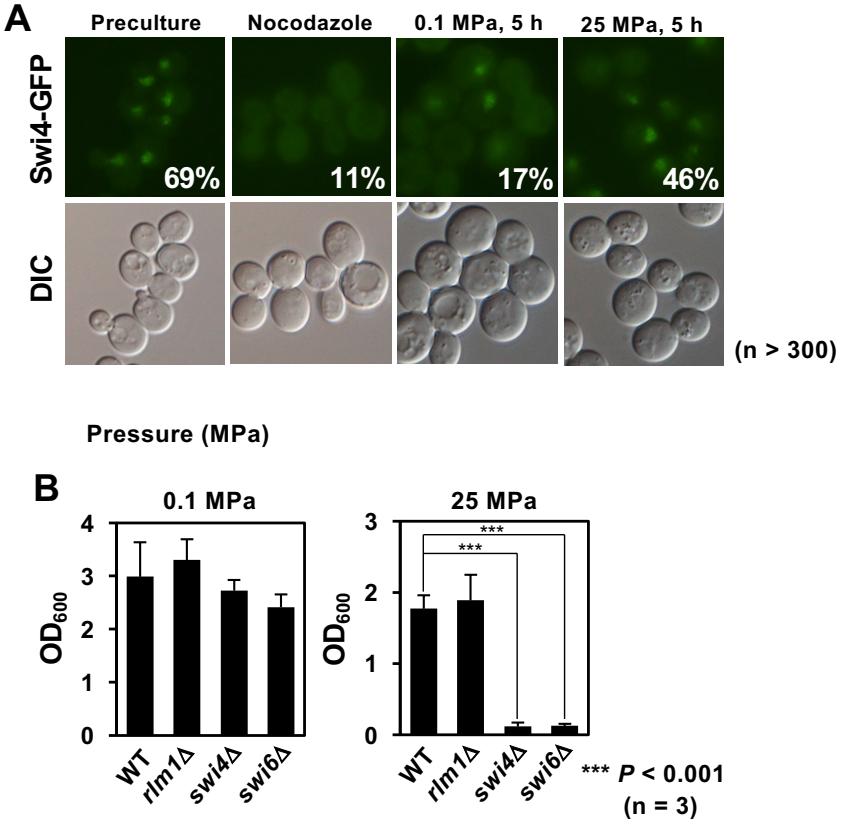

Fig. 4. Mochizuki *et al.*

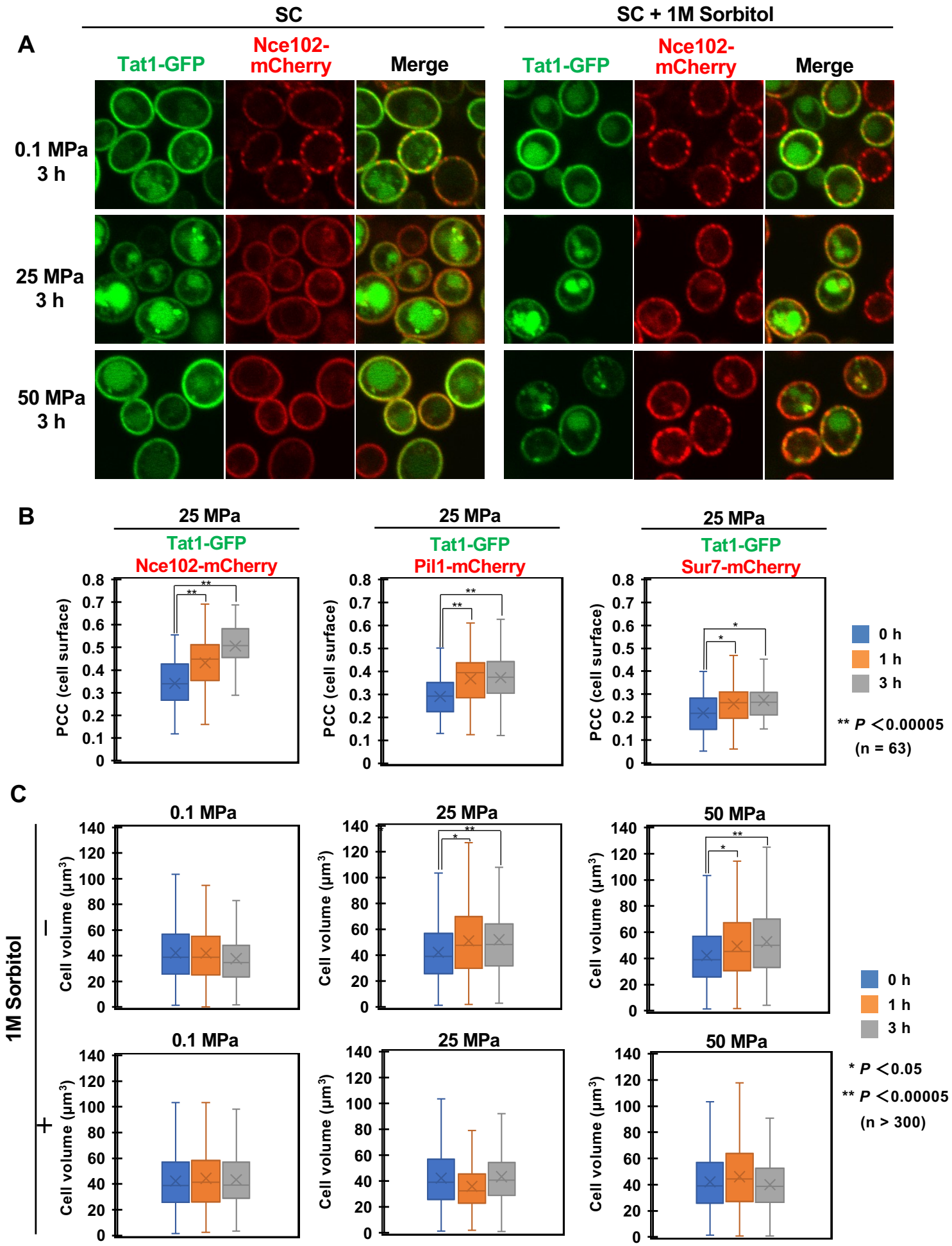

Fig. 5. Mochizuki *et al.*

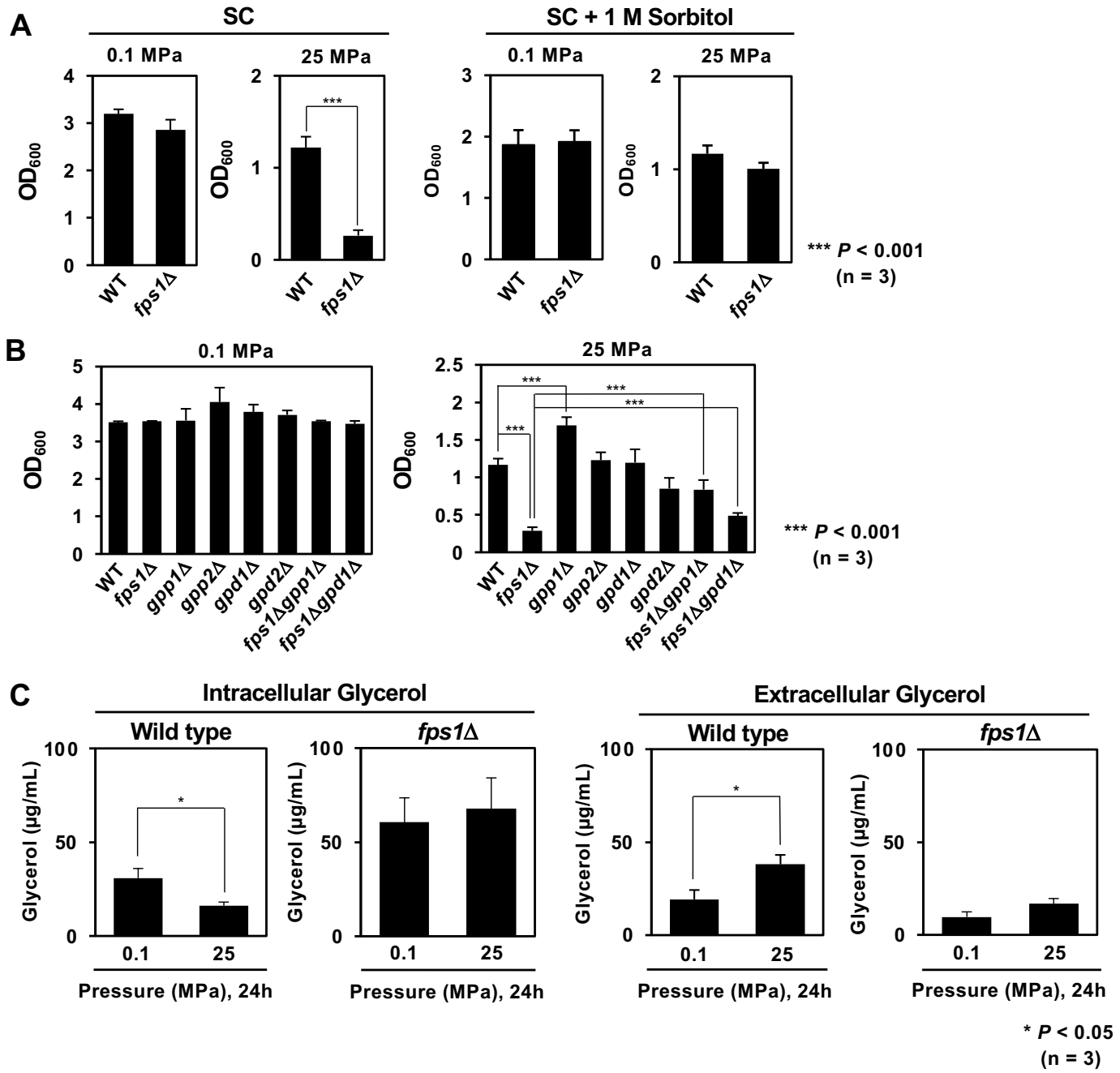

Fig. 6. Mochizuki *et al.*

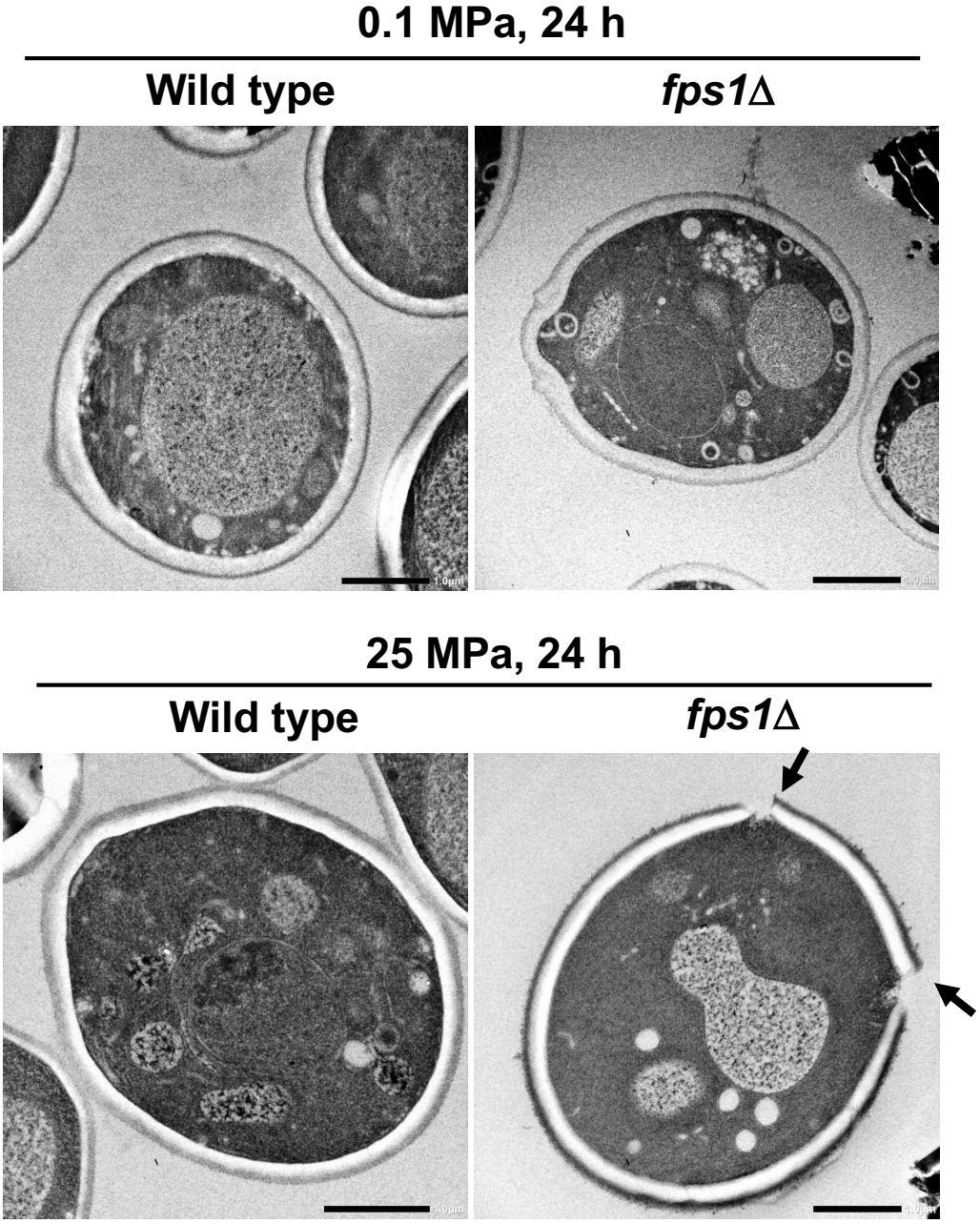

Fig. 7. Mochizuki *et al*.

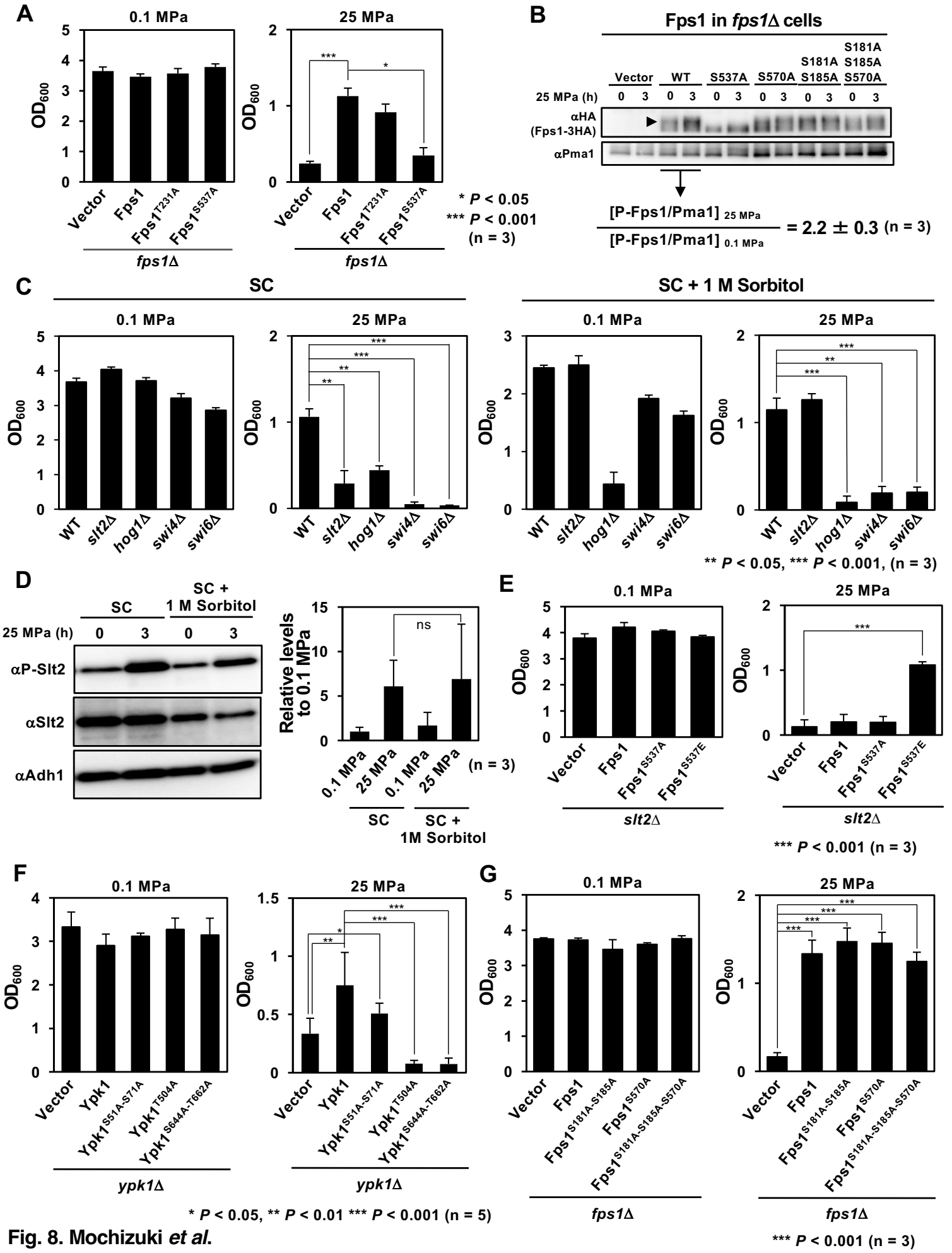

Fig. 8. Mochizuki *et al.*

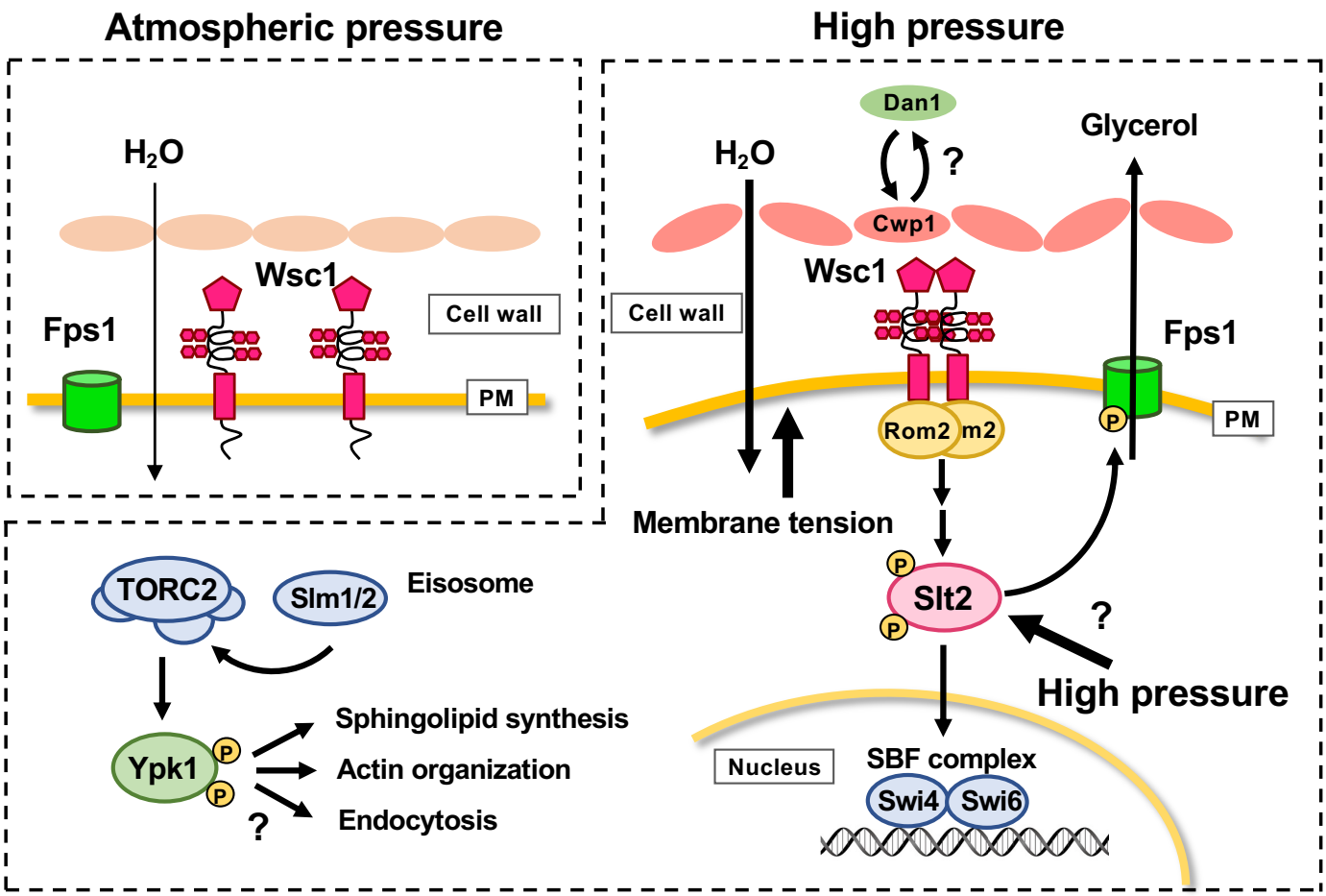

Fig. 9. Mochizuki *et al.*

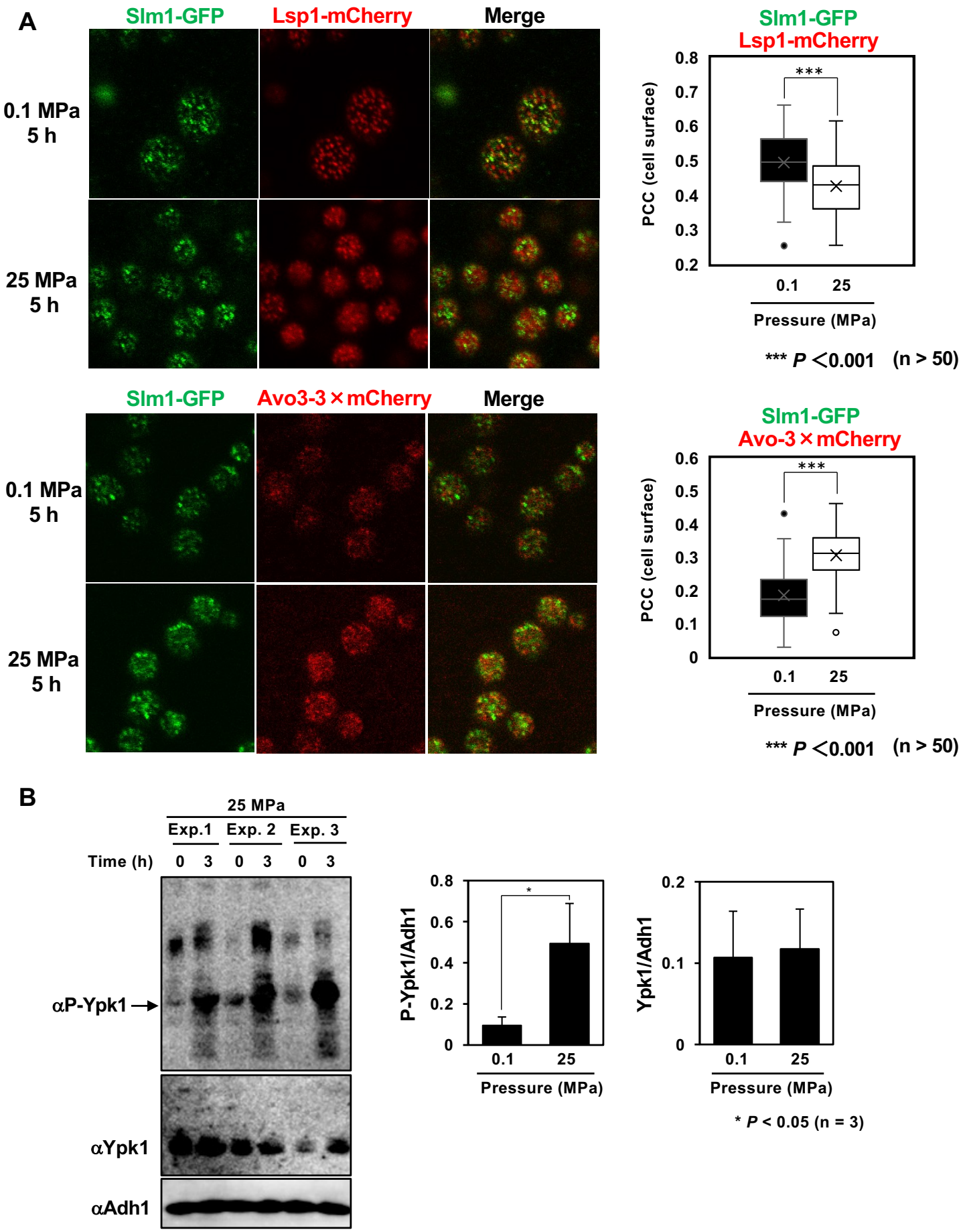

Fig. S1. Mochizuki *et al.*